The influence of thermal noise on Liesegang pattern formation

And other related aspects of this remarkable phenomenon.

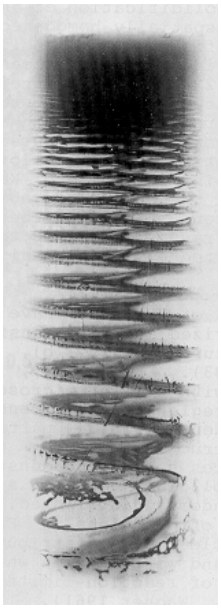

Nicolas Chevalier

ITP - EPFL

Under the supervision of : M.Droz, I.Bena, Ph-A.Martin

24th of February 2006

Contents

Acknowledgments

I would like to express my gratitude to all the people who have helped me in writing this diploma thesis : Prof. M. Droz, Dr. Ioana Bena, and Prof. Zoltán Rácz.

Enoncé du travail

Etude théorique des structures de Liesegang dans le cadre d'un scénario de décomposition spinodale.

Dans ce travail de diplôme, le candidat étudiera certains aspects nouveaux de la formation des structures de Liesegang. Se basant sur le formalisme de décomposition spinodale introduit dans l'article PRL 28, 2880 (1999), le candidat étudiera les problèmes suivants :

1. Influence du bruit stoschastique sur la formation des structures.

   Dans l'étude faite dans la référence ci-dessus, les fluctuations sont absentes. Le candidat étudiera d'une part comment introduire les fluctuation thermiques dans le modèle de décomposition spinodale et d'autre part, quels en sont les effets sur la formation des structures.

2. Formation des structures de Liesegang en présence d'un champ électrique.

   Un développement récent dans l'étude des structures de Liesegang concerne le comportement en présence d'un champ électrique extérieur. Le cas où les ions impliqués dans la formation du front de réaction-diffusion a été étudié récemment dans les articles J.Chem Phys 122 024512 (2005) et J. Chem Phys. 122, 204502 (2005). Expérimentalement, il se trouve que l'un des ions dans la réaction est bivalent. Le candidat généralisera les résultats ci-dessus au cas de ions bivalents.

Remarque du candidat : les réponses aux questions posées dans l'énoncé correspondent principalement aux chapitres 4, 5 et 6 du présent travail. C'est dans ces mêmes chapitres que se trouvent les quelques contributions authentiques de l'auteur.

Chapter 1

Liesegang rings

1.1 A prototypical experiment

R.E. Liesegang (1869-1947) was the son of a wealthy phototechnical industrial, P.E. Liesegang. It is in the cosiness of the family's own laboratory that the discovery of what is now known as *Liesegang rings* came about.

> "Die Schicht wurde diesmal nicht getrocknet, sondern im feuchtem Zustand, also als Gallerte benutzt [...] Als das Chlornatrium in der Gallertschicht durch doppelchromsaures Kali ersetzt wurde, zeigte das in den aufgesetzten Silbernitratstropfen nach einem Tage entstandene rote Silberchromat ein vollkommenes anderes Bild : Statt des geschlossenen Chlorsilberkreises waren es zahlreiche rote Ringe, die durch klare Zwischenräume unterbrochen waren. Gleich beim ersten Blick dieser rythmischen Erscheinung war die Gewissheit da, dass es sich um etwas Besonderes, vielleicht Neues, zumindest um etwas bisher zu wenig Beachtetes handele.[1]"

Since Liesegang's first encounter with these rings, the experiments were reproduced in a whole variety of different setups, with different geometries

[1]"This time on, the paper hadn't been dried, but kept in a humid state, as a gel [...]. Did the Natrium Chloride in the gel be replaced by $K_2Cr_2O_7$, and a drop of $AgNO_3$ added on top of the solution, so did the emerging red $AgCr_2O_7$ precipitate show up in a drastically different shape : instead of the closed AgCl disk, numerous red rings had formed, separated by clear blank spaces. It became clear from the very first glance at these periodic Erscheinungs, that this was something peculiar, maybe something new, well at least that hadn't until now attracted sufficient attention. "

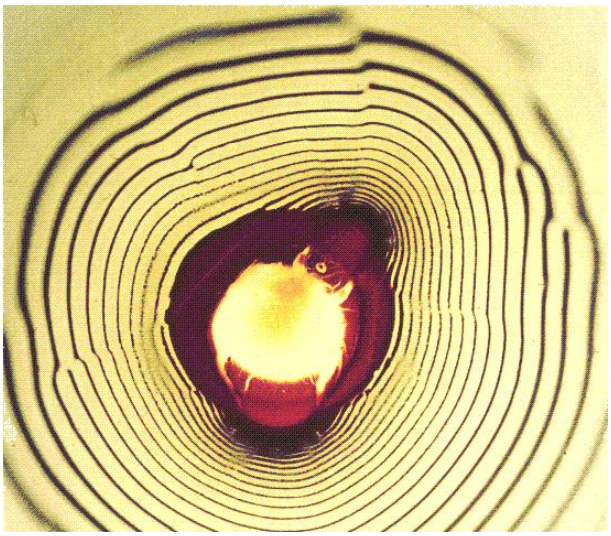

Figure 1.1: (a) The typical experiment that Liesegang could have performed, involving the formation of a dark $Ag_2Cr_2O_4$. The highly irregular form of the drop induces defects.

and chemical compounds. Fig.(1.1) shows the typical result of such an experiment.

While the ring formation was the first to be observed, we shall be talking in this work mostly of bands, by reference to the experiments performed in test tubes, and to the schematic setup depicted in Fig.(1.2). We will call this a "1D" experiment since it involves only one relevant direction[2].

1.1.1 Relevant scales

Typical concentration-, time- and length- scales are given below :

- the overall length of the pattern is $l_{exp} \sim 0.2$ m
- the overall time of its formation is $\tau_{exp} \sim 1 - 2$ weeks
- the width of the bands increases from a first-band value $w \sim 1$ mm to a final-band value $w \sim 1$ cm

[2]The following abbreviations will be often used in the text : LP for Liesegang pattern, LE for experiment, LR for rings.

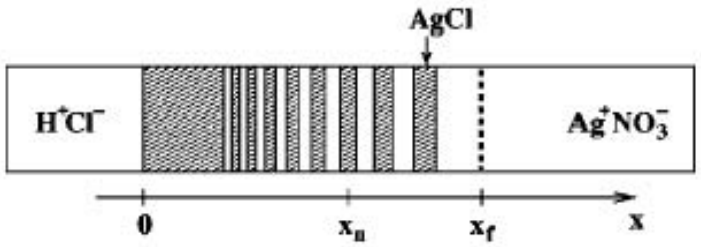

Figure 1.2: Schematic picture of a typical 1-dimensional Liesegang experiment. The correspondence with the notation in the text is given by $A^- = Cl^-$, $A^+ = H^+$ (outer electrolyte); $B^+ = Ag^+$, $B^- = NO_3^-$ (inner electrolyte); and $C = AgCl$ (precipitate). The initial interface between electrolytes is at x = 0. The precipitation bands (shaded regions) emerge in the wake of the moving reaction-diffusion front (dashed line at x_f).Each band can be moreover characterized by its width w_n.

- typical diffusion coefficients for ions in gelatine are $D_f \sim 10^{-9}$ m^2 sec^{-1}. We shall see later that the reaction front may be characterized by its own diffusion constant which is approximately 10 times that of the ions.

- the first bands form within a time $\tau_{band} \sim 30 - 60$ min

- typical concentrations are of the order of $a_0 \sim 1$mol L^{-1} and $\frac{a_0}{b_0} \sim 100$. The more concentrated reactant we will call the *outer electrolyte* (A) while the other one will be the *inner electrolyte* (B).

1.1.2 The four generic laws and further observations

The following experimental facts may be observed :

1. the distance at which the n-th band appears obeys the so-called *time-law* :

$$x_n \propto \sqrt{t} \tag{1.1}$$

   This law is satisfied in all the experiments where it was measured and it appears to be a direct consequence of the diffusive dynamics of the reagents.

2. the distance between consecutive bands forms a geometrical series, which can be resumed in the following *spacing-law*:

$$x_n \approx Q(1+p)^n \tag{1.2}$$

The quantitative experimental observations concern mainly this law.

3. More detailed works go past the confirmation of the existence of the geometric series and study the dependence of the spacing coefficient on a_0 and b_0. Q denotes the amplitude of the spacing law and p is given by the *Matalon-Packter* law :

$$p = F(b_0) + G(b_0)\frac{b_0}{a_0} \tag{1.3}$$

where F and G are decreasing functions of their arguments.

4. The fourth and last generic observation is the *width-law*:

$$w_n \approx x_n^{\alpha} \tag{1.4}$$

where α is close to 1.

This is the least established law since there are problems with both the definition and the measurement (fluctuations) of the width. Recent, good quality data does support, however, the validity of (1.4).

A last generic feature that is observed in most experiments is the appearance of a *plug* at the interface between the outer electrolyte and the gel. It is a zone of continuous precipitate, or at least where the band structure is so small that it can't be distinguished by the naked eye.

Among the data which can't be termed as generic, but would certainly be of help for the establishment of a quantitative theory, is the measurement of the concentration of the precipitate (that is, in the various bands) in the system after formation. The only available data on this point is given was given by Zrinyi (private communications) for tubular experiments and indicates the following : from the plug to approximately the middle of the system, the density in the bands climbs up to a maximum, and then falls back with increasing band number. The overall variation in concentration is of small amplitude.

They moreover notice the presence of precipitate ($\approx 5\%$ of that contained in the bands) in the inter-band spaces.

1.1.3 Morphological changes

Perfect concentric Liesegang rings are obtained only in the frame of very neat experiments as the one designed by Obrist (1937) (see [18], Fig.(1.3)).

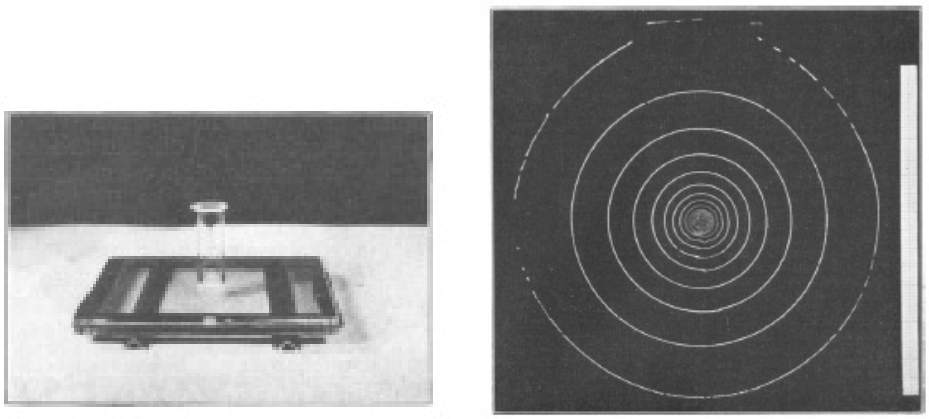

Figure 1.3: The following setup (a) was designed by J.Obrist and allows for the formation of very regular concentric rings (b). Two glass plates cover the gel from above and below, inhibiting its drying. The tube in the middle contains the outer electrolyte, thus providing a steady source of A, in contrast to a simple drop.

Most of the time, inhomogeneities in the gel, changes in temperatures, impurity of the chemicals used, etc. lead to interesting morphological changes of the resulting pattern. These observations are of particular importance to us since fluctuations (noise) should be to some degree responsible for them. Simulations including noise might thus give insight in the causes of such defects, or shall we rather say, ornaments. Fig.(1.4) shows three different kinds of anomalies which seem to be encountered frequently in various LEs. The spiral which serves as a cover illustration for this work is also a typical, reproducible defect.

It is shown in [10] that many of the morphological defects presented here can be reproduced from simulations with particular initial conditions : for example, a 2D spiral was observed to form as a result of the highly irregular form of the drop of outer electrolyte they implemented. In a rectangular geometry, anastomose was shown to be a consequence of edges (steps) in the initial distribution of the outer electrolyte.

Let us also mention the occurrence of *inverse banding*, where the bands were observed to build up in the reverse order, that is getting closer and closer to each another with time. *Secondary banding* refers to the observation that bands break up into several little sub-bands.

One should emphasize that such behaviours, though of great interest, are very system specific and can't be expected to emerge in the frame of a general model. In this thesis, we will thus mainly be concerned with the reproductible facts, that is the four laws, and the "generic" defects presented in Fig.(1.4).

1.2 Conditioning a Liesegang experiment

Here, we wish to discuss the various conditions under which a Liesegang experiment can be carried out. We will point out the (numerous) important external parameters.

On the gel

The gel is an important component of LP formation. It inhibits *convection*, allowing for pure *diffusion* of the electrolytes. In fact, the "plug" (ie continuous precipitate formation) observed at the beginning of most of the experiments is caused by hydrodynamic convection effects of the liquid drop. Indeed experiments performed by [20] where the outer electrolyte is also contained in a piece of gel (a sort of sponge) shows a radical shrinking of this plug; impressively thin bands form from the very beginning of the process.

So what is a gel ? A common way of preparing *gelatine* is for example to dissolve proteins in water at a high enough temperature and let the solution cool down (a string of events which naturally takes place when you fry a chicken). The proteins build up a loosely interconnected network, while water permeates it as a continuous phase. A typical classification criterion of the jelly obtained is its resistance to sheer. There exist many types of gels but the two main ones used for LE are *agarose* and *silica* gels. The role of the coagulant is played in the first by long carbonated sugar strings extracted from seaweed (a submarine plant, alga) . In the second it is monosilicic acid H_4SiO_4. Typically, one has at hand some Na_2SiO_3 which, dissolved in water, gives us :

$$Na_2SiO_3 + 3H_2O \rightleftharpoons H_4SiO_4 + 2NaOH$$

H_4SiO_4 is then able to polymerize with the liberation of water, giving rise to a network of Si-O links (see Fig.(1.5)).

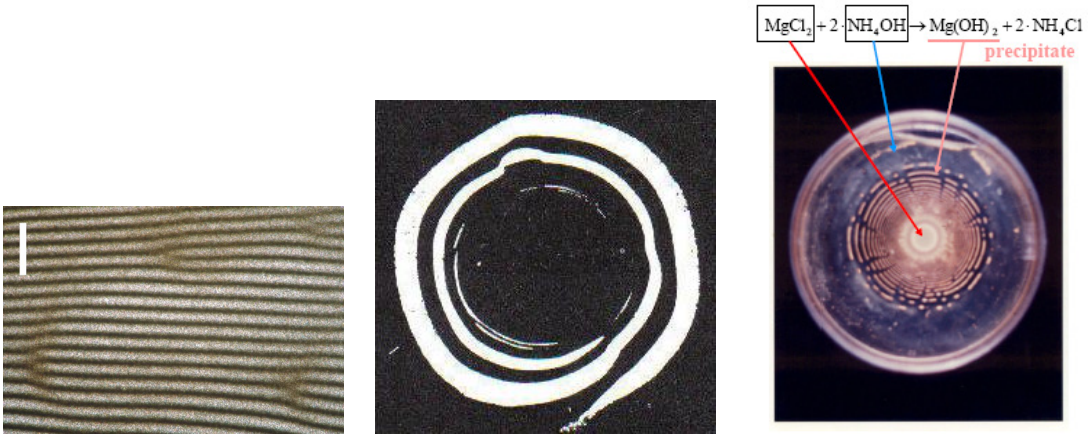

Figure 1.4: (a) Blow up of a defect known as "anastomose", the non-matching of bands at an intersection, CuO system, from [32] (b) Spiral formation obtained by R.E.Liesegang himself([31]). (c) The appearance of blank alleys in the precipitate can be seen. Rings are most often not closed.

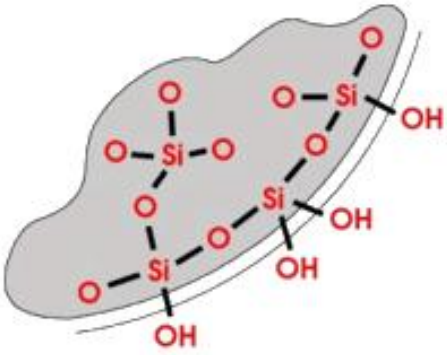

Figure 1.5: Schematic view of the structure of a silica gel.

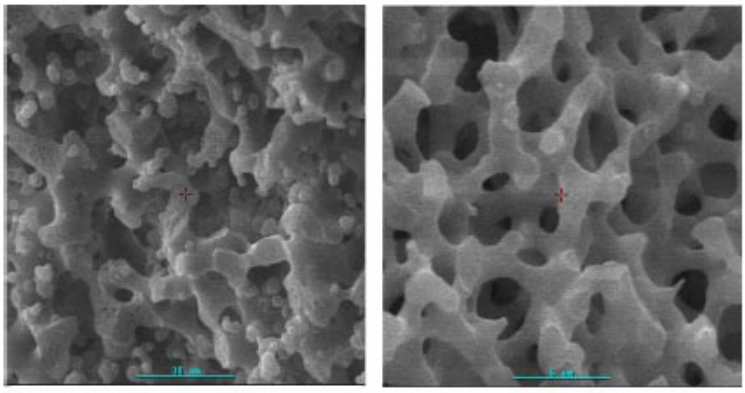

Figure 1.6: Scanning electron microscopy (SEM) of a silica gel. The blue bar measures 6 μm in both pictures, but the composition of the gel differs from one to the other, resulting in different pore size.

Fig.(1.6) gives a microscopic view of what a real gel looks like. One sees from the picture that an important characteristic is the average *pore size*: it has been reported that, while electrolytes diffuse in gels, colloids, which are bigger, often do not. This effect is used in the method of gel electrophoresis for separating molecules of different volumes.

We said that a gel allows for diffusion: from the above microscopic snapshot, it is however not clear that Einstein's picture of water molecules hitting randomly the electrolytes (which causes them to perform a random walk) is not hindered or modified by the labyrinth-like structure of the gel. Actually, the existence of restricted paths in the way a molecule may perform its random walk is the starting point of *sub-diffusion* theories, which predict - among other - a slower scaling law for the average distance traveled in a time t ($\sqrt{x^2} \propto t^\alpha, \quad 0 < \alpha < 1/2$) than the one of diffusion [21].

However, we do not expect these modifications to be of importance for our purpose. The multiple confirmations of the time-law do seem to indicate that diffusion is the process through which particles move in a gel.

The reactants

The nature of LPs depends a lot on the reactants used. Fig.(1.7) shows 3 examples of tubular Liesegang experiments with different species. The crystalline structure of the compound formed is clearly visible in some cases while it isn't (at least to the naked eye) in others. Note that the tendency to form

Figure 1.7: (a) Mixed Liesegang and dendrite formation in agarose gel, PbI precipitate, from [33]. The low concentration in gel molecules is responsible for this behaviour. (b) Bands of silver chromate (note the striking difference with Fig.(1.1), due probably to the more tender gel structure used here). (c) System of calcium phosphate.

amorphous rather than crystalline precipitate is also strongly dependent on the structure of the gel used.

It is to expect that most of the electrolytes which can form a visible precipitate should be able to produce LP (see below the example of Liesegang rings in urea, an organic compound). One (among many) counterexample should however balance this statement: $Fe_4[Fe(CN)_6]_3$ (also known as the "prussian blue" dye) precipitate happens to act like a semipermeable membrane, accumulating at its surface $Fe(CN)_6^{4-}$ but letting through Fe^{3+} ions LP formation would accordingly not happen if $Fe(CN)_6^{4-}$ were the outer electrolyte.

P. Hantz [32] investigated the CuOH system and found out that LP is only one of a whole manifold of possible patterns in the space of the initial concentrations of the outer and inner electrolyte (a_0, b_0).

In the remainder of this thesis, we will refer to systems exhibiting the most simple kind of behaviour such as the dichromate potassium or silver nitrate ones, which were also abundantly used in the experiments reporting the four laws (1.1.2).

Effect of an electric field

It was shown experimentally that a constant electric field applied to the system has considerable effect on the pattern formation. This is important since it is an external parameter that is easily controlled and can thus be used to shape LPs. One reports the following observations for an electric field pushing the precipitating ions towards each other :

1. The appearance of a uniform precipitation for sufficiently high field-intensities and/or after a sufficiently long time.

2. There is an "acceleration" of the band formation, i.e., the time of appearance of the first band decreases with increasing field intensity.

3. A decrease of the spacing between successive bands (as compared to the fieldless case) with increasing field intensity.

These observations point out an important fact: the particles responsible for the formation of the precipitate cannot be considered as neutral if we are to apply an electric field. We have to take into account their dissociation into ions and the resulting force generated by the electric field in their equation of motion. We will tackle this point in the last part of this work, Chap.6.

Shedding light on Liesegang rings

Submitting a LE to the irradiation of visible light was found to have quite prominent effects. The number of rings formed within a given time period was generally found (see [17]) to be increased compared to systems which remained in darkness. Other authors didn't report any effect of light. This must ultimately depend on the chemical species used (we know for example that some precipitates undergo chemical transformations when subjected to light, i.e., the darkening of AgCl) and on the gel. It is for example known that Cr^{2+} ions (involved in the reaction of Liesegang's first experiment) subject to light can transform in Cr^{6+}. In some cases, this ion can crosslink gel molecules (the monosilicic acid we talked about), making the gel a more rigid one, thus diminishing the diffusion constants of the ions, which should ultimately bring up consequent changes in the resulting pattern.

Placing ourselves in a perspective to *control* Liesegang pattern formation, light could be a very useful tool in as far as it is clean (it doesn't require adding new species and can be turned on and off at wish); it would allow to locally alter the diffusion constants of the ions.

Temperature dependence

Though this section could be considered as the experimental counterpart of our thesis's title, no thorough experiment has been performed concerning such a dependence. Liesegang reports that "a cooler room is better than a hot one", a fact that one can intuitively agree with. It would actually have little sense to do such an experiment since too many parameters would simultaneously vary with temperature: diffusion coefficients, reactions rates, precipitation thresholds, etc.

1.3 Liesegang rings in nature

Periodic patterns are ubiquitous in nature. Liesegang rings however aren't, that is, they seem to appear only in a fairly narrow window of parameters. The fact that convection currents should be avoided is probably the most stringent restriction since they would otherwise be prone to develop on the surface of liquids. Moreover, the concentration ratio between the outer and inner electrolyte should be high enough and this is not an easy condition to meet in natural systems. Nevertheless, several appearances of stripy things were interpreted on ground of the LP formation.

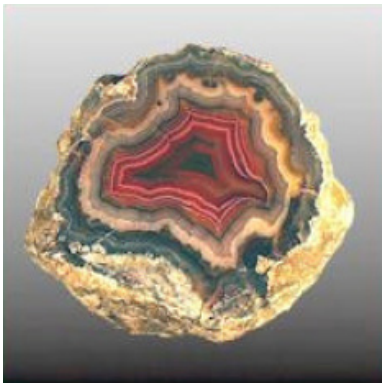

Figure 1.8: An agathe rock (also called "serpent's egg") : the stripes are remniscient of Liesegang rings.

Agate rocks

This first example seems to have made its way through the scientific community's acceptance. The idea was proposed by R.E.Liesegang himself. Some examples of agate rocks are shown in Fig.(1.8).

One clearly sees that the bands seem to get closer to each other as we reach the center of the rock.

The mechanism for their formation is thought to go as follows : a long time ago, these rocks were not rocks at all, but a soup of silica, water, and other materials resting in the bosom of vulcanic cavities. This soup would eventually jellify, thus permitting substances outside the cavity to diffuse into it : inverse banding LP formation could then settle. Once all striped, the gel would solidify and end up in the state we know.

At first sight, this sequence of events seems like a true incarnation of faith. For our poor knowledge of the subject, criticism here would be all but misplaced; we refer the reader to the existing literature.

The structure of the solar system

This is certainly the most audacious - if not exuberant - hypothesis built on LP. Authors Toramaru et al. noticed [36] the striking similarity between the Titus Bode law - according to which the planets's distances to the sun follow a geometrical series - and the spacing law of LPs. On this basis, they constructed a model in which the whole mass of the solar system is initially distributed at its center and diffuses in the surrounding nebula. Ensuing chemical reactions would then lead to LP and thus to a solar system satisfying

the Titus Bode law.

While this model is fun, it certainly neglects a good deal of important details like the gravitational forces at play, and the exact nature of the "chemical reaction" taking place.

And in other places

Liesegang rings were also found to form in mortar deposits, where the role of the gel is played by clay or packed sand. Characteristic banding appearing in geological structures were also reported as being of the Liesegang type.

Concentric ring structures were observed in the spreading of mushrooms and bacterias on a food substrate and are thought to be of the Liesegang type, see Fig.(1.9).

Finally, let's mention the (annoying) occurrence of Liesegang rings in the bladder where they can built up (though not in the same magnificent way as they do in test tubes) from urea, as kidney stones do.

1.4 Epilogue to the introduction

In his late years, Liesegang retired to a small country house in the outskirts of Frankfurt. He shared the place with Dr.Hanf-Dressler, a physician and her daughter Heide. The latter draws a quick portrait of her guest in her child's memories :

> "Hoch augerichtet und gravitätisch mit seiner unverzichtbaren "Melone" auf dem Kopf und einem Gänseblümchen im Knopfloch, schritt er durch Wiesen und Felder. Er war schon eine bemerkenswerte Gestalt in dieser Umgebung. [3]"

Having swirled through the experimental aspects of Liesegang phenomena and hopefully lighten up some of the reader's curiosity, we invite him to follow, in an attempt to elucidate the matter, along the steps of this odd-looking rambler.

[3]Tall and solemn with his indispensable "melon" on the head and a daisy in the buttonhole, he roamed through fields and meadows. He certainly was a noteworthy figure in the surroundings.

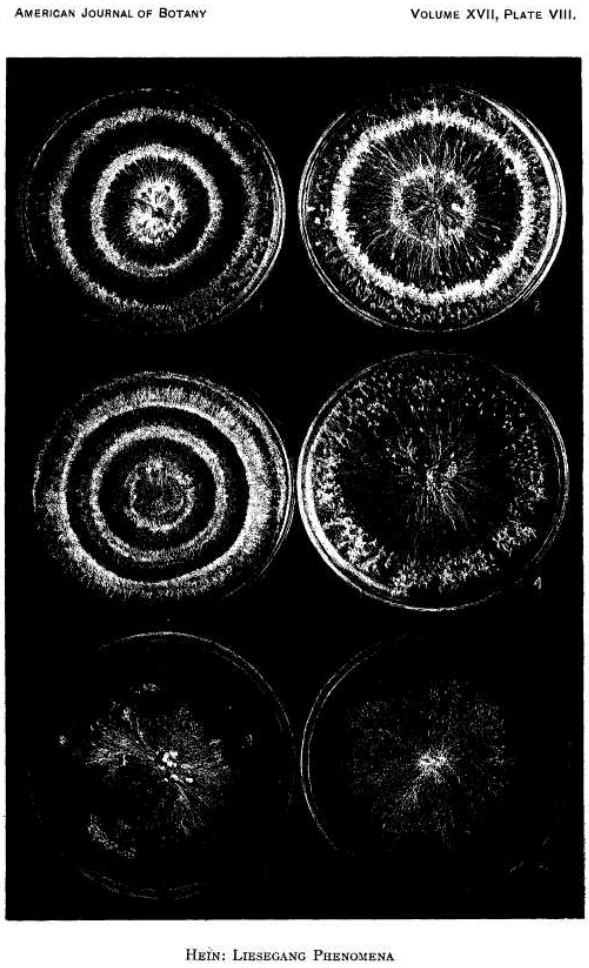

Figure 1.9: Liesegang rings obtained from the growth of fungi on a nutrient gel, from [35].

Chapter 2

A basic understanding

In this chapter, we wish to present the basic physics hidden behind Liesegang phenomena. Before rushing to the next paragraph, we strongly encourage the reader to sketch an explanation for himself : why rings, and not mere precipitate puddle ? Besides making this reading a more rewarding activity, it should also equip the reader with sharper criticism towards the inanities we may be exposing.

2.1 Supersaturation theory

2.1.1 The mechanism

We consider here the case of 1D Liesegang bands. The mechanism, summarized in Fig.(2.1) goes as follows : A being much more concentrated than B, it will invade the gel. As A diffuses in the gel, it reacts with B and creates a precipitate. Precipitation doesn't spontaneously occur upon contact of the reactants: the latter have to exceed a given supersaturation threshold, given by the solubility product $[Ag^+][Cl^-] = ab = K'_S$. The ' on K'_S refers to the "super-" of supersaturation. In fact, it is known that in medias where the mixing of the species A and B is slow (like in gels), precipitation will not immediately occur when $ab = K_S$. The gel can be *supersaturated* (that is, in a metastable state) up to a value $K'_S \gg K_S$[1]. Once K'_S is reached, Ag^+ and Cl^- transform to the solid precipitate form $AgCl$ until their concentrations reach the lower (equilibrium) value $[Ag^+][Cl^-] = K_S$. We have a local *depletion* of the surrounding electrolytes, the whole region where we had $[Ag^+][Cl^-] > K_S$ contributes in the formation of a precipitation zone.

[1] K'_S depends strongly on the gel, the purity of the chemicals and dishes used, temperature, and is thus difficult to evaluate experimentally.

After precipitation, the gel is, in this depletion zone, no more supersaturated, and we consider as an hypothesis that the precipitation band doesn't hinder further diffusion of the electrolytes. So the A's continue to diffuse outwards. Having past the limits of the previous depletion zone, the concentrations will eventually come to a point where they can once again allow for precipitation, leading to the creation of a second band, and on goes the diffusion front...

In the frame of this picture one can talk about a *quasi-periodic precipitation and depletion cycle*.

The presence of a threshold (which, as we will see, occurs in all theories of Liesegang phenomena) is clearly demonstrated in an experiment done by Zrinyi, see Fig.(2.2).

This simple picture is known as a *supersaturation* (or *prenucleation*) theory and, as we will see shortly, accounts for most (but not all) of the salient features of LP formation.

2.1.2 Analytical formulation

The initial conditions and the dynamics of A's and B's are given as follows before any band formation has yet happened :

$$\begin{aligned} \dot{a}(x,t) &= D_A \triangle a(x,t) \\ \dot{b}(x,t) &= D_B \triangle b(x,t) \end{aligned} \tag{2.1}$$

$$\begin{aligned} a(x,t=0) &= a_0 \theta(-x) \\ b(x,t=0) &= b_0 \theta(x) \\ a_0 &\gg b_0 \end{aligned} \tag{2.2}$$

The condition for precipitation of band number $n+1$ at time t_{n+1} is :

$$a(x_{n+1}, t_{n+1}) b(x_{n+1}, t_{n+1}) = K'_S \tag{2.3}$$

Moreover we know that this will happen at the maximum of the bell-like curve ab, so we add the condition :

$$\frac{\partial}{\partial x}(a(x_{n+1}, t_{n+1}) b(x_{n+1}, t_{n+1})) = 0 \tag{2.4}$$

The depletion mechanism is taken into account by stating that band number n acts as a sink for the minority species (B), that is $b(x_n, t) =$

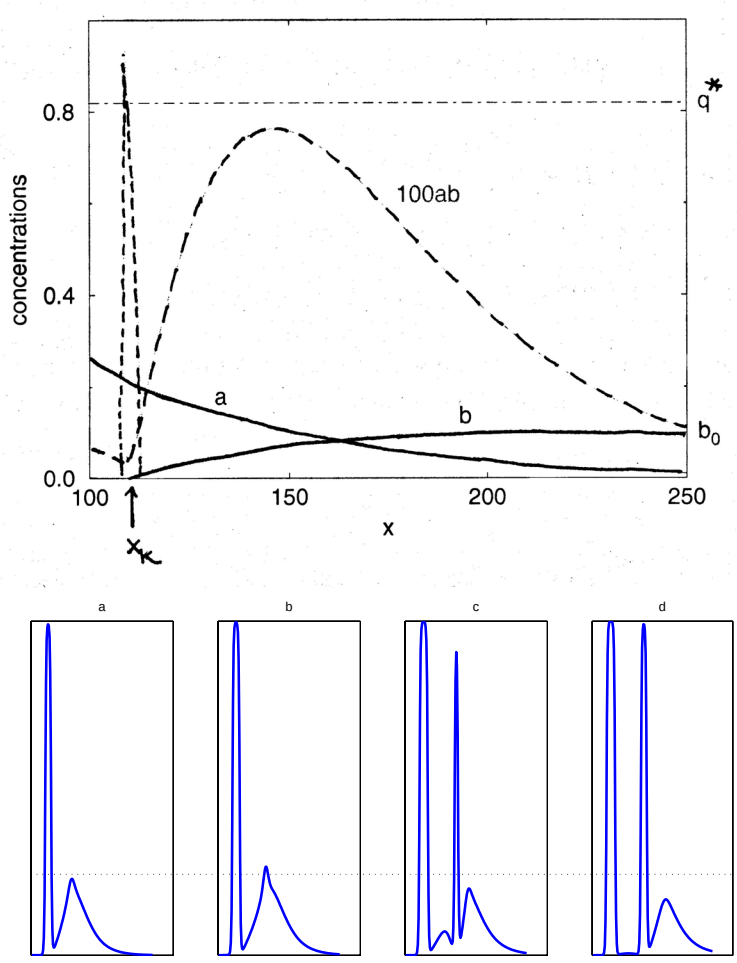

Figure 2.1: The first scheme represents the typical curves described by $a(x)$, $b(x)$, $a(x)b(x)$ after the formation of band k, q^* being the supersaturation threshold. In the second scheme, we see a typical precipitation-depletion cycle. The thick line indicates the value of the ionic product kab. The dotted line indicates the supersaturation threshold. In the theory formulated by Ostwald (and Prager), the bands are said to be infinitely thin and form instantaneously upon crossing of the threshold.

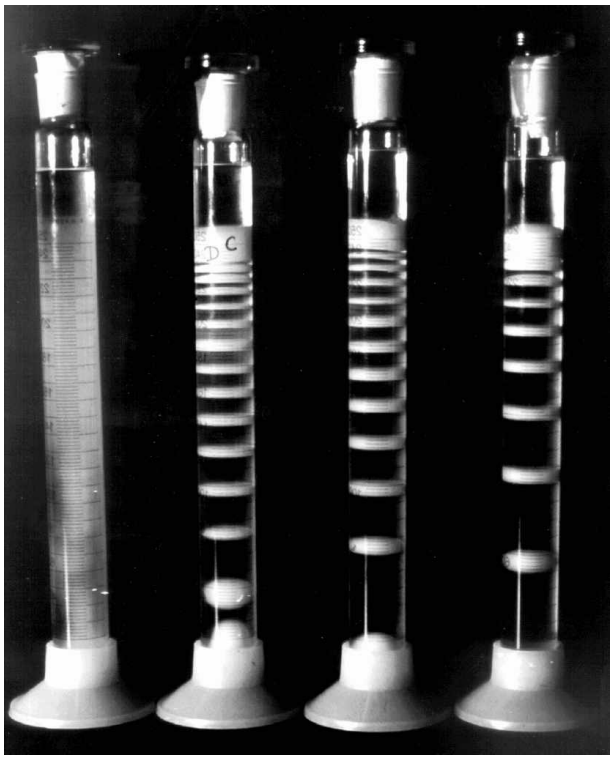

Figure 2.2: Patterns obtained with A= NaOH and B= $MgCl_2$ in polyvinylalcohol gel. The white precipitate is C=$Mg(OH)_2$. The columns show different patterns due to the different initial concentrations of A. In the first tube from the left, the concentration is too low and no pattern appears, clearly demonstrating the existence of a threshold below which patterning does not occur. The Matalon Packter law says that p decreases with increasing a_0. So the the order of increasing a_0 in the tubes should be 1,4,3,2.

$\sqrt{K_S}$. Since K_S is very small compared to the concentrations at play, and namely to K'_S, we put $b(x_n, t) = 0$. The A's are assumed to be unaffected by the precipitate formation (since $a_0 \gg b_0$). For $t_n < t < t_{n+1}$, solving the equations (2.1) with these boundary conditions, we get :

$$\begin{aligned} a(x,t) &= a_0 \mathrm{erfc}\left(\frac{x}{\sqrt{4D_A t}}\right) \\ b(x,t) &= b_0 \mathrm{erf}\left(\frac{x - x_n}{\sqrt{4D_B(t - t_n)}}\right) \end{aligned} \tag{2.5}$$

Replacing these equations in (2.3), (2.4) leads to a system which can be solved numerically for the quantity p defined as

$$\frac{x_{n+1}}{x_n} = 1 + p$$

We *assume* that there exists a spacing-law and test whether it admits solution. The details of this (numerical) derivation are given in [4] and give the following expression for p :

$$p = 0.02 + 5\sqrt{\frac{D_B}{D_A}}\frac{K'_S}{a_0 b_0} \tag{2.6}$$

This is the Matalon-Packter law, which, since p is (bless the Lord) not dependent on n, also proves the spacing-law. We see that as the concentrations a_0 and b_0 get bigger, the bands form closer (more equidistant) one to another. If moreover, the A species would diffuse much faster than the B's, one would expect almost equidistant banding.

The time-law in this theory is a direct consequence of the purely diffusive motion of the species, whose profiles are always functions (named here below f_1, f_2, $f = f_1 f_2$) of $x/\sqrt{t}$ so (2.3) can be written :

$$\begin{aligned} f_1(\frac{x_n}{\sqrt{t_n}}) f_2(\frac{x_n}{\sqrt{t_n}}) &= K'_S \\ \leftrightarrow f(\frac{x_n}{\sqrt{t_n}}) &= K'_S \\ \leftrightarrow x_n &= f^{-1}(K'_S)\sqrt{t_n} \propto \sqrt{t_n} \end{aligned} \tag{2.7}$$

Derivation of the width-law necessitates supplementary knowledge about the total amount of precipitate produced. We will present this derivation in the more natural frame of nucleation and growth theory.

2.2 Nucleation and postnucleation theory

It is often observed that a diffusion (or more precisely reaction-diffusion) front travels through the gel leaving behind itself a haze of a characteristic color ([13], [32]), which can be viewed as a colloidal suspension. This lead to the development of *nucleation and growth* and *postnucleation* scenarios. Both assume the existence of a species C (the haze) resulting from the reaction $A + B \rightarrow C$, which, through its own specific dynamics, leads to band formation. Nucleation and growth relies basically on the same ideas as supersaturation theory but gives a more detailed picture of the precipitation process. Postnucleation appeals to an intrinsic instability of the deposited colloidal suspension. In both cases, supersaturation theory is relegated to providing the colloidal suspension of C's through the product kab.

Nucleation and growth can be embodied in the set of equations :

$$\begin{aligned} \dot{a}(x,t) &= D_A \triangle a(x,t) - ka(x,t)b(x,t) \\ \dot{b}(x,t) &= D_B \triangle b(x,t) - ka(x,t)b(x,t) \\ \dot{c}(x,t) &= D_C \triangle c(x,t) + ka(x,t)b(x,t) - \text{"nucleation and growth"} \\ \dot{d}(x,t) &= \text{"nucleation and growth"} \end{aligned} \tag{2.8}$$

where D is the final, immobile substance from which the bands are formed. The C's are nucleation seeds, that is the base product from which precipitation can occur.

What we call the "nucleation and growth" term is a non-linear term describing precipitation. It could be a simple threshold like $\theta(c - K'_S)$ or something more sophisticated describing how solid nucleation centers emerge and grow by surface aggregation (we will come back to this approach in Chap.4). Through this mechanism, computer simulations with equations of the type (2.8) yield bands with a valid spacing-law.

Postnucleation theory can be embodied in the set of equations :

$$\begin{aligned} \dot{a}(x,t) &= D_A \triangle a(x,t) - ka(x,t)b(x,t) \\ \dot{b}(x,t) &= D_B \triangle b(x,t) - ka(x,t)b(x,t) \\ \dot{c}(x,t) &= \text{"non-linear dynamics"} + ka(x,t)b(x,t) \end{aligned} \tag{2.9}$$

In this theory, it is the "non-linear dynamics" term which will give rise to banding (the source term being still kab), i.e., we hope the solution profile

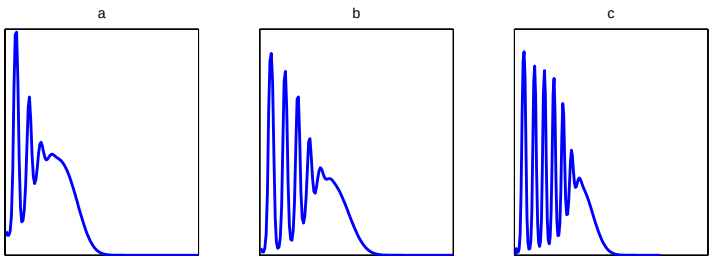

Figure 2.3: In the simulation of this postnucleation theory, the deposited suspension of C's breaks up into several bands as a result of an instability. Though the mechanism of formation is different from supersaturation/nucleation and growth theories, it is hard to say from a simple look at the resulting pattern which of the two is at play.

of (2.9) for $c(x,t)$ will present distinct high and low density regions. This term should, in addition to describing the diffusion of the C's, also describe aggregation, which might lead to band formation. [13] explains band formation in the frame of such a theory, borrowing their non-linear term from the Lifschitz-Slyozov late stage growth theory. The theory on which the present work is based (which will be exposed throughout Chap.3 and 4) belongs to the postnucleation type.

Fig.(2.3) illustrates a possible post-nucleation behaviour : the front is seen to break up immediatly in several bands as a result of an instability.

2.2.1 The spacing law in the (post-)nucleation picture

The spacing law admits a simple derivation which relies on the numerical observation of the C in the system, see Fig.(2.4). We suppose the reaction rate infinite. At the reaction point, if n is big enough so that B doesn't limit the reaction, we have $|j_A| = |j_C|$.

In the simplest kind of nucleation theory, precipitation of the band occurs when c reaches a threshold c^*. Let us evaluate the particle currents (derivatives) according to Fick's law (refer to Fig.Fig.(2.4)) :

$$\begin{aligned} j_A &\approx D_A \frac{a_0}{x_{n+1}} \\ j_C &\approx D_C \frac{c*}{x_{n+1} - x_n} \end{aligned}$$

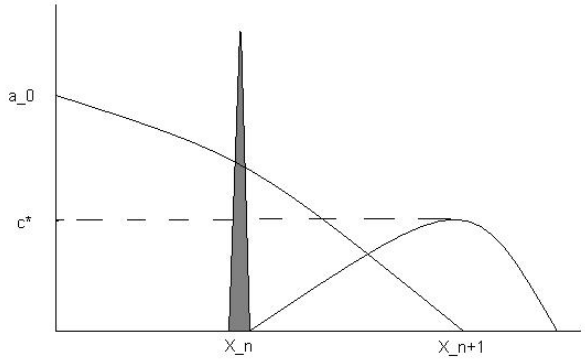

Figure 2.4: Schematic view of the concentration profiles of A (almost straight curve starting from the very left) and C (bell like curve), illustrating the derivation of the Matalon-Packter law in a postnucleation theory.

Such expressions are only valid for large band number n (i.e., large distances from the source), where we can approximate all diffusive profiles by straight lines. Combining these with $|j_A| = |j_C|$, we get

$$1 + p = \frac{x_{n+1}}{x_n} = 1 + \frac{D_C c^*}{D_A a_0} \tag{2.10}$$

This shows both the spacing (since p is not dependent on n) and the Matalon-Packter law ($p \sim \frac{1}{a_0}$). However, since the B were not considered in this argument, we can't hope to find the dependence on b_0 which enters in (1.3).

2.2.2 The width-law

It will be shown in Chap.3 that, if the precipitate were an immobile inert product, the reaction would deposit *a constant quantity* c_0 of it per unit length. It is observed that most of the C turns up into one of the precipitate band, while a little of it, say c_l, stays in the interband region. From the experimental data presented in Chap.1, the densities in and out of the bands can be taken to be roughly constants c_h, c_l. It is then easy to see that if the bands have ever greater distances between them and the conservation of C

is to hold, than the bands have to increase in width. More quantitatively, denoting by w_n the width of band n, conservation of C requests:

$$(x_{n+1} - x_n - w_n)c_l + c_h w_n = c_0(x_{n+1} - x_n) \tag{2.11}$$

which, together with the spacing law, yields the amplitude λ of the width-law.

$$w_n = p\frac{(c_0 - c_l)}{(c_h - c_l)}x_n = \lambda x_n \tag{2.12}$$

We have thus shown that the spacing law implies the width-law. One may of course object that the argument also applies to supersaturation theory; we agree, but the fact is just that supersaturation theory doesn't provide any motivation for calculating the amount of precipitate produced. Consequently, it is not a surprise that this simple argument first appeared in the frame of post-nucleation theories.

Other aspects of the pattern formation appear as a result of post-nucleation. For example, R.Feeney et al. [13] claim that secondary banding is a consequence of competitive particle growth inside a band, and that inverse banding can also be obtained from such models.

2.3 Conclusions

Supersaturation is the minimal model for explaining Liesegang patterns. Nucleation and growth and post-nucleation models are more realistic and manage to explain the width-law. The viewpoint we will defend in this work is the following : nucleation and post-nucleation are two aspects of a phase transition, which can be described in a unique model (see Chap.4). In the next chapter, we will attack the problem of knowing how the C is produced by the reaction-diffusion front.

Chapter 3

Kinetics of diffusion limited chemical reactions

In the frame of this work, we will opt for a theory where some kind of intermediate species C is formed, which could be interpreted, for instance, as a colloidal suspension. It is the dynamics of this suspension which will be responsible for the banding process; this will be the object of the last two parts of this work.

In this chapter, we wish to explain how the formation of the C's comes about. We know from our general chemistry courses that

$$Ag^+ + Cl^- \rightleftharpoons AgCl\ |_{solid} \tag{3.1}$$

The $\rightleftharpoons$ indicates that the reaction should, in all generality, be considered as reversible, thus allowing for redissolution of the colloidal suspension. In a saturated solution at equilibrium (where some precipitate is already present), the remaining ionic concentrations satisfy

$$[Ag^+][Cl^-] = K_s \tag{3.2}$$

where K_s is the solubility constant. For AgCl, $K_s = 1.610^{-10}\mathrm{M}^2.\mathrm{L}^{-2}$ at 25°C, so that precipitation occurs at low values, $[Ag^+] = \sqrt{K_s} \approx 10^{-5}$. Typical values of K_s range between 10^{-5} and 10^{-15} $\mathrm{M}^2.\mathrm{L}^{-2}$. Since our order of magnitude for concentrations is $b_0 \approx 0.1$ $\mathrm{M.L}^{-1}$, formation of the colloidal suspension happens at, relatively, low concentrations and the remaining ions from the equilibrium (3.1) can be neglected. We will thus consider the following schematic reaction :

$$A^+ + B^- \rightarrow C \tag{3.3}$$

An ionic gel solution of (A^+, A^-) and (B^+, B^-) is neutral up to distances corresponding approximately to the Debye screening length $r_D = \sqrt{\frac{\epsilon_r \epsilon_0 RT}{F^2 n_0}} \sim 10^{-9}$ m. This expresses the fact that any positive ion is surrounded by an assembly of negative ions which exponentially reduces the electrostatic potential created by the first above distances corresponding to r_D. . The diffusion length-scale of interest to us being typically $x \sim \sqrt{2D \quad 1\text{sec}} \sim 10^{-4}$m, we will ignore the ionic nature of the ions, boiling down (3.1) to

$$A + B \rightarrow C \tag{3.4}$$

Let us point out that the electric charges carried by A and B have to be taken into consideration in two cases :

- When the diffusion coefficients of A's and B's are different. This is pointed out in [24]. In fact, after the reaction (3.3) occurs, the remaining ions A^- and B^+ have to recombine in order to guarantee that the gel is everywhere neutral. This constraint generates forces when the mobility (diffusion coefficients) of the ions are not the same.
- When electric fields are present.

Both aspects are presented in more details in the last chapter of this thesis.

In a typical Liesegang setup (see Fig.(1.2)), the reactants are initially separated and $a_0 \gg b_0$ which leads to the propagation of a *reaction-diffusion front* along the concentration gradient. Knowing the properties of this front is a problem of considerable interest whose solution will be presented here below.

3.1 The reaction-diffusion front

The case presented in Fig.(1.2) with the reaction (3.4) can be embodied in the set of equations :

$$\begin{aligned} \dot{a}(x,t) &= D_A \triangle a(x,t) - k a(x,t) b(x,t) \\ \dot{b}(x,t) &= D_B \triangle b(x,t) - k a(x,t) b(x,t) \\ \dot{c}(x,t) &= k a(x,t) b(x,t) \end{aligned} \tag{3.5}$$

$$\begin{aligned} a(x, t=0) &= a_0 \theta(-x) \\ b(x, t=0) &= b_0 \theta(x) \end{aligned} \tag{3.6}$$

$$c(x, t=0) = 0 \tag{3.7}$$

where the C species is taken to have no dynamics at all for the time being (none of the non-linear terms present in (2.9) or (2.8)). Indeed we wish to concentrate first on how much and how the C is deposited by the reaction. The reaction kinetics have been modeled by the usual kab term with k the reaction constant. Well, how "usual" this term is, is actually a more delicate question than might be expected at first sight. We will come back to this issue in the second part of this chapter.

3.1.1 Motion of the center of the front

We consider the simplified case $D_A = D_B$ (numerical computation showing no qualitative departure from this case for unequal diffusion constants). A first step in solving this set of non-linear PDEs involves the density difference $u = a - b$, which satisfies a simple diffusion equation $\dot{u} = \triangle u$. With the boundary conditions (3.6) the solution can be quickly shown (by use of Green's function most efficiently) to be :

$$u = \frac{1-q}{2} - \frac{1+q}{2}\mathrm{erf}\left(\frac{x}{2\sqrt{t}}\right) \tag{3.8}$$

with $q = b_0/a_0$. We got rid of all other parameters by measuring length, time and particle density in units of, respectively, $l = \sqrt{D/(ka_0)}$, $\tau = 1/(ka_0)$ and a_0.

We expect the reaction to be some sort of bump (since no reaction takes place where reactants are missing, at the far right and the far left), whose maximum is reached at the only "singular" point of the system, x_f, defined by $a(x_f, t) = b(x_f, t) \leftrightarrow u(x_f, t) = 0$ (f stands for "front"). Indeed at this point the exact stoechiometry of the reaction is respected.

This picture is confirmed (or was inspired by) numerical resolution, see Fig.(3.1). Two length-scales appear : the depletion width W_d, where the values of a and b are significantly smaller than their initial values, and the reaction width w where the product $R = kab$ takes a significant value. As k increases, w gets smaller and the reaction zone more and more resembles a delta-peak.

The resolution of $u(x_f, t) = 0$ yields

$$x_f(t) = \sqrt{2D_f t} \tag{3.9}$$

where D_f is the effective diffusion constant of the front defined as the implicit solution of

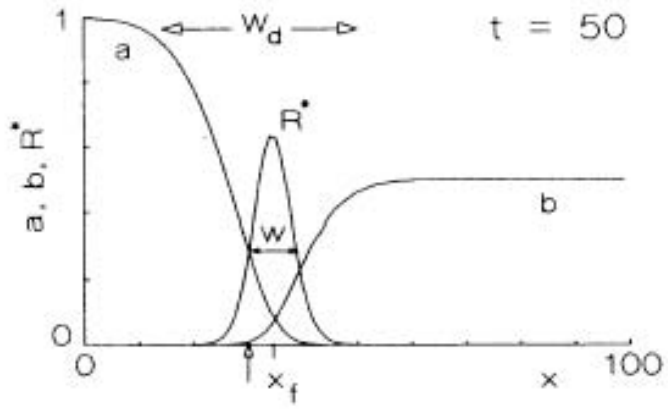

Figure 3.1: Numerical solution of (3.5) with the boundary conditions (3.6). $R^*(x,t) = kab$, which will be approximated by a gaussian $S(x,t)$ in the remainder of the text, is the rate of formation of C's. The simulation demonstrates that the reaction rate is maximum where $a = b$. Moreover, one sees that the width of the front w is much smaller than the depletion zone W_d. From [23].

$$\text{erf}\left(\sqrt{\frac{D_f}{2}}\right) = \frac{1-q}{1+q} \tag{3.10}$$

Equation 3.9 is an important step since it relates to the *time-law* (1.1). It confirms that, in spite of the reaction taking place, the dynamics is still (effectively) diffusive.

3.1.2 The reaction rate and the width of the front

The two other quantities of interest are the rate of the reaction and the width of the front.

One could continue by replacing the solution for u in the equation for a but the equation we get

$$\dot{a} = a'' - a^2 + ua$$

is impossible to solve exactly. Its scaling behaviour for $t \to \infty$ was studied in [23]; we will just content ourselves with a simple physical argument which

reproduces the same results.

Let's suppose that

$$\begin{aligned} w &\approx t^{\alpha} \\ R &\approx t^{-\beta} \\ W_d &\approx t^{1/2} \end{aligned}$$

The last equation can be obtained if we consider the front as a sink ($a(x_f) = 0$), a source of A at $x = -\infty$, and solve the corresponding diffusion equation. The slope of $a(x,t)$ is then at long times $\frac{\partial a}{\partial x} = \frac{a_0}{W_d} \approx t^{-1/2}$.

The number of C particles created in a unit time is then :

$$\int_{\substack{reaction \\ zone}} \frac{\partial c}{\partial t} \quad \propto t^{-\beta+\alpha} \tag{3.11}$$

But on the other hand the reaction rate is also equal to the current of either two of the species to the reaction zone, $j_A = \frac{\partial a}{\partial x} \mid_{x_f} \approx W_d^{-1} \propto t^{-1/2}$. So we get the first relation : $-\beta + \alpha = -1/2$.

To get a second relationship, we note that we can integrate the relationships $j_A = \frac{\partial a}{\partial x} \mid_{x_f} \sim t^{-1/2} \sim j_B$ over the reaction zone to get an approximate idea of the number of A's and B's in it. We thus have $a \sim b \sim wt^{-1/2} \sim t^{\alpha-1/2}$. Then $R = kab \sim t^{2\alpha-1}$ and we get $2\alpha - 1 = -\beta$. Solving this system yields

$$\alpha = 1/6 \quad \text{and} \quad \beta = 2/3 \tag{3.12}$$

Being in possession of the necessary exponents, it can be shown numerically (see Fig.(3.1)) that the reaction rate $R(x,t) = kab$ is very well approximated by a Gaussian, which we will name $S(x,t)$ (for Source), i.e.

$$S(x,t) = \frac{A}{t^{2/3}} \exp\left(-\frac{(x - x_f(t))^2}{2w(t)^2}\right) \tag{3.13}$$

with

$$\begin{aligned} w(t) &= \frac{2\sqrt{D}t^{1/6}}{(ka_0K)^{1/3}} \equiv w_0 t^{1/6} \\ K &= \frac{b_0}{a_0 2\sqrt{\pi}} \exp\left(-\frac{D_f}{D}\right) \\ A &= 0.3ka_0^2K^{4/3} \end{aligned}$$

Thus the production rate of C' (i.e., the reaction rate) can be entirely expressed as a function of the initial concentrations a_0 and b_0, their diffusion constants D_A and D_B and of the reaction rate k.

A limiting case of importance is the one of *infinite reaction rate*, $k \to \infty$. The front then reduces to a δ-peak separating an A-free (right) from a B-free region (left). If we reproduce the preceding argument with $\alpha = 0$, we find $\beta = 1/2$ and the front can be shown to obey

$$S_\infty(x,t) = a_0 K \sqrt{D} \frac{\delta(x - x_f(t))}{\sqrt{t}}$$

We shall retain the expressions of $S(x,t)$ and $x_f(t)$ as the two major results of this section.

3.1.3 Quantity of precipitate deposited by the front

Last, but not least, comes an important conclusion concerning the density of C's produced by the reaction : it is found to be *constant*.

Let's consider a fixed small interval of time dt, which corresponds to the front moving a distance $dx = \dot{x_f}(t)dt \sim (1/\sqrt{t})dt$. The number of C particles deposited in this small interval will be equal to the current of one of the two reactants times dt. This current is, for the diffusive case $j \approx 1/\sqrt{t}$. Thus $\#c = dt/\sqrt{t} \sim dx$ and $\#c/dx \equiv c(x) = c_0$ where c_0 is a constant approximately equal to the concentration of the minority reagent B.

The exact expression for the concentration of C's left behind the front is:

$$c_0 = a_0 K \sqrt{\frac{2D}{D_f}} \tag{3.14}$$

3.2 Doubts and shivers concerning the $-kab$ term

Without throwing over the results presented in the preceding section, we intend to show here that writing reaction-diffusion equations in the form (3.5) may oversee some of the physics of the problem and lead to incorrect results.

The concern is about concentration fluctuations, which are absent in (3.5). It is indeed an equation for the concentration of A's which is averaged over

the fluctuations. In analogy with critical phenomena (such as Weiss's theory of magnetism), (3.5) are termed *mean-field* equations. Now imagine that in a volume V, we initially have the homogeneous concentrations $a(x,0) = b(x,0) = a_0$. The reaction rate is everywhere the same and we should have $a(x,t) = b(x,t) = a(t) = b(t)$ everywhere, so that $\triangle a = \triangle b = 0$. The RD-equations thus reduce to

$$\frac{\partial a(t)}{\partial t} = -ka(t)^2 \tag{3.15}$$

which admits the solution

$$a_{\substack{mean\\field}}(t) = \frac{a_0}{1+kt} \propto \frac{1}{t} \tag{3.16}$$

But if we take in account fluctuations, the picture changes drastically from the very beginning: imagine than in a given region, $a(x,t)$ has fluctuated so that after the reaction has taken place in this region, B dominates. The whole space will then be divided in alternating A- and B-rich regions as can be seen in Fig.(3.2).

The reaction will only take place at the *interface* between those regions, and we henceforth expect the decrease of A (or B) to be much slower than the $\frac{1}{t}$ behaviour predicted by mean-field. The reaction is clearly limited by the diffusion. If the diffusion constants were infinite, every particle would have an equal chance of reacting with any other particle (like in a gaz), and we expect the mean-field behaviour to be recovered.

As fluctuations have settled a regime in which A's and B's are separated in domains, we see that the $D_A \triangle a(x,t)$ terms will contribute strongly to the dynamics at the interfaces, while the fluctuations might only play a negligible role. So in this regime, there is still hope for the equations (3.5) to be valid. In fact, the initial conditions in which the reactants are placed have an important impact on the outcome of the problem : we will in the following treat the cases of *homogeneous reaction-diffusion* as opposed to *reaction-diffusion with initially separated reactants*. The latter corresponds to the Liesegang setup. We will see that *dimension* plays a critical role in determining whether (3.5) are valid or not.

3.2.1 The homogeneous case

A complete scaling argument is given in [1], we will only give here its pictorial version. Since we felt the argument sufficiently limpid in its original version,

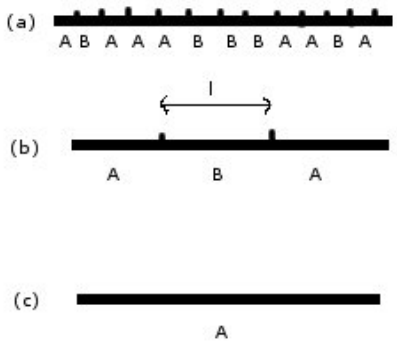

Figure 3.2: Schematic illustration of the domain-growth process. (a) Initially randomly distributed A's and B's. (b) Mixing over a length $l \approx (Dt)^{1/2}$. (c) Domain coalescence.

we quote directly from [1] :

> Let's consider a volume $V = l^d$, containing $N_A = a_0 l^d \pm \sqrt{a_0 l^d}$ particles, where the second term represents the fluctuations. After a time $t \approx l^2/D$, the particles will have time to "mix" within the volume V and annihilate in pairs leaving only the residual fluctuations. These residual particles define a domain in which the number of particles is simply $\sqrt{\rho_A(0) l^d}$, or equivalently a particle density of $\sqrt{\rho_A(0)/l^d}$ as illustrated in Fig.(3.2). Since the system is a homogeneous collections of alternating A-rich and B-rich domains, each of size $l \sim (Dt)^{1/2}$, the global density is approximately one half the density within a single domain. We therefore conclude that $\rho_A(t) = \sqrt{\rho_A(0)}(Dt)^{-d/4}$.

3.2.2 The heterogeneous case

In the case where the reactants are initially separated, we intuitively expect fluctuations to be less important for the reaction kinetics than in the homogeneous case. A theoretical argument supporting this fact is to be found in [2], which finds that the limiting dimension as from which the mean-field equations are valid is reduced to $d = 3$. For $d_{critical} = 2$, there are logarithmic corrections to the mean field rate.

Simulations (see [22]) moreover confirm that this critical dimension is 2.

3.3 Conclusions

1. Since all LP experiments done so far always took place in three dimensions, the results presented by the mean field theory of [23] are applicable to the description of the reaction front. One should though bear in mind that we simplified the reaction to $A + B \rightarrow C$, which might not always be a good approximation.

2. One of the main goal of this diploma work consists in evaluating the influence of thermal noise on LP formation. In a theory where the dynamics of the C (in contrast to a supersaturation theory) will be responsible for the appearance of rings, the role of the A and B species is relegated to providing the system's source of C's. Since a mean-field description of this source is correct, *the only relevant stochastic term left to add are the fluctuations in the density of C's.*

Chapter 4

The dynamics of precipitation

We all know from our basic chemistry courses that there exists a limiting concentration known as the *saturation threshold* above which the ionic species are no more dissolved in the solvent (ie the gel, or water), but crystallize to precipitate form. The freezing of water or the appearance of a spontaneous magnetization in ferromagnetic materials also exhibit such threshold-behaviour (for temperature); they are all examples of transitions between different phases.

The main hypothesis of Ostwald's (among other's) theory is that the concentrations locally exceed a threshold. Such a state is termed *metastable* because it will inevitably undergo precipitation under the effect of small perturbations (fluctuations). Examples include supercooled water or the freezed magnetization of a magnet below its phase transition temperature.

We see that a simulation of LP formation which goes beyond the hypothesis of infinitely thin bands requires us to model the dynamics of precipitation. This chapter will present the basic notions necessary to grasp this phenomena.

4.1 Metastable and unstable states

Let us consider a system composed of two phases. We place ourselves far away from the critical point so that the transition is a first-order one.

The nearest-neighbour ferromagnetic Ising model [26, 27] is the archetype of such systems and will often be quoted in the following sections; the reader

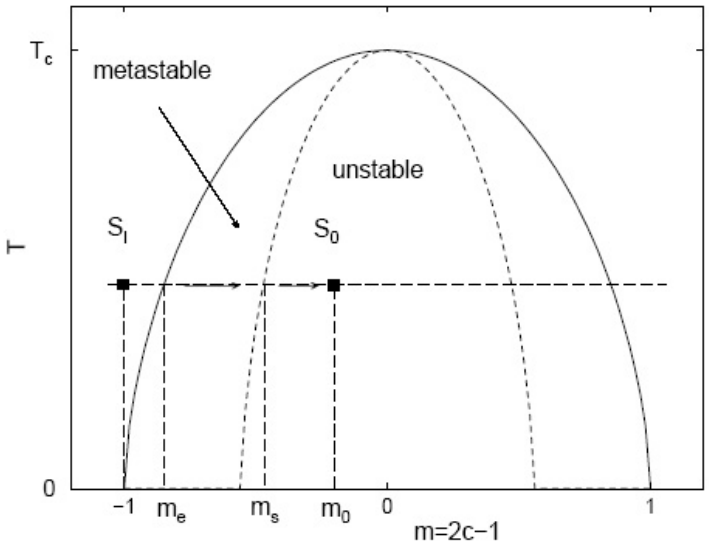

Figure 4.1: Qualitative phase diagram for the Ising model. The magnetization m is related to the density c of C particles through $m = 2c - 1$. The solid line is the coexistence curve and the dotted one is the spinodal line.

should just bear in mind the equivalence spin-down $\leftrightarrow$ no precipitate, spin-up $\leftrightarrow$ precipitate to make the link with our initial supersaturation issues.

The phase diagram of the Ising model is given in Fig.(4.1). The dotted line is called the spinodal line and is defined in the frame of a mean-field theory such as Weiss's one : it corresponds to the points where $\frac{\partial^2 f}{\partial m^2} = 0$, where f denotes the free energy of the system. The zone where $\frac{\partial^2 f}{\partial m^2} < 0$ is termed the unstable zone since the system is thermodynamically unstable. Any perturbation will induce phase separation. The zone where $\frac{\partial^2 f}{\partial m^2} > 0$ is the metastable zone : the system is still thermodynamically stable, but it would be energetically favorable to phase separate. The phase separation in this case requires overcoming an energy barrier, as will be explained in more detail in the following section.

It should be emphasized that this delimitation is only a mean-field one, the transition being continuous from one regime to the other when taking into account fluctuations. But the spinodal nevertheless does describe an important physical difference in the transition from these zones to an equilibrium (two-phase coexistence) situation, as will be made clear below.

4.2 Nucleation and Growth

4.2.1 Nucleation

A metastable state decays to equilibrium by *nucleation and growth*. Let us suppose we have an equilibrium situation with a positive (upwards directed) magnetic field. We quickly switch the field to a negative one, quenching the system in a metastable state. The system would be in equilibrium by flipping its spins downwards. These emerge from the background metastable phase as droplets (just as condensation droplets form when a gaz is sudddenly cooled). We can describe the transition to equilibrium by a description of the rate at which droplets of size l of down-spins, $n(l)$. In order to create such a droplet, one has to overcome an energy barrier $E(l)$ so we can use Boltzmann statistics to say that

$$n(l) = N\exp(-\beta E(l)) \tag{4.1}$$

where N is a normalization coefficient, $E(l)$ is the energy of a single droplet and $\beta = 1/k_B T$. Note that this last expression is only valid for small enough and dilute droplets whose formation is statistically independent of the other ones. Otherwise it would predict that $n(l) \to \infty$ as $l \to \infty$ (see Fig.(4.2)), which is clearly unphysical. Moreover we assume that we somehow continuously suppress the bigger droplets so that an equilibrium situation can be reached where $n(l)$ is constant in time. The energy consists of two terms :

$$E(l) = \underbrace{2Hl}_{\substack{bulk\\ term}} + \underbrace{\sigma l^{(d-1)/d}}_{\substack{surface\\ term}} \tag{4.2}$$

where d is the dimension of the system. The first term favors the growth of such particles since $H < 0$. On the other hand, the second one, describing a surface tension with the other surrounding up-spins, tends to decrease the number of small droplets. A plot of the free energy is found in Fig.(4.2).

We see that there is a critical size l_c as from which droplets of down spins are energetically favorable and grow. But this requires a big enough fluctuation, or, in other terms, an *activation energy*. We can associate to this activation energy a typical nucleation time τ_{nucl} for the system to transit from a metastable state to equilibrium.

The equivalent free energy for a 3D precipitate/solute system would be, if we take r to be the radius of the droplet,

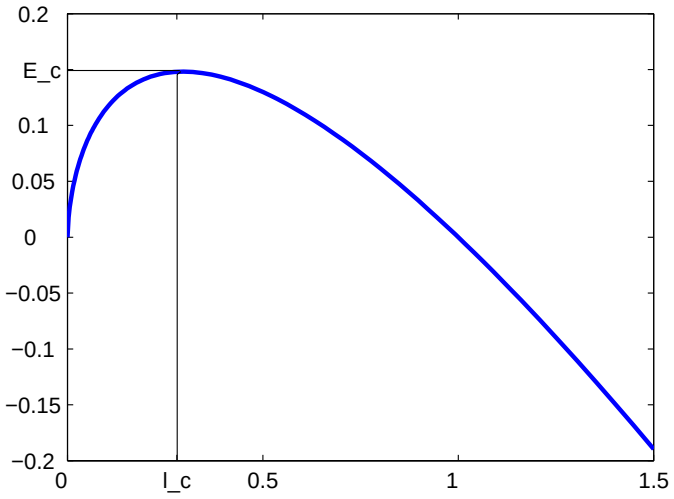

Figure 4.2: Plot of the free energy of (4.2). One sees that there exists a critical size l_c (denoted r^* for the precipitate/solution case) as from which droplets are energetically favorable and grow.

$$E(r) = -\frac{4}{3}\pi r^3 \Delta f + \sigma 4\pi r^2 \tag{4.3}$$

where $\Delta f > 0$ is the difference in free energy per unit volume of the precipitate compared to the solute phase. The relation of Δf to the supersaturation is given by the so-called Gibbs-Thomson formula:

$$\Delta f = kTln\left(\frac{c}{c_\infty}\right) \tag{4.4}$$

where σ is the surface tension, c the local concentration and c_∞ the concentration at which droplets would have to be of "infinite" radius to nucleate. (c/c_∞) is thus a measure of the supersaturation, and plays the role of the magnetic field in the bulk term of 4.2.[1]

By combining Eq.(4.3) and (4.4), one can obtain the dependence of the critical radius on the supersaturation :

$$r^* = \frac{w}{ln(c/c_\infty)} \tag{4.5}$$

[1]More detail on the derivation of this relation can be found in [31]; the idea is to compute the change in free energy along an isothermal path going from the initial metastable point in the phase diagram to the point corresponding to the coexistence of both phases.

where w is a constant.

We call this transition scheme more precisely *homogeneous* nucleation to differentiate it from *heterogeneous* nucleation where alien bodies (impurities) provide the necessary seeds for phase transition. Heterogeneous nucleation is typically observed in champaign (and other fizzy drinks) where thin residual tissue filaments in the glass provide centers for the nucleation of CO_2 bubbles.

4.2.2 Growth

Now that the crystal seeds have nucleated, how do they grow ? The answer to this question depends on the kind of system considered, so we will focus here on precipitating solutions. The following argument is presented by Dee ([5]).

The C particles diffuse : as they encounter a seed, we may say they aggregate to it since it has (at least) the critical size. The rate at which particles diffuse from a distance d to a given point is D/d^2. Since there are $c(x,t)4\pi r^{*2}d$ particles in a shell of size d around a nucleus, we may write the growing rate $\Gamma(c)$ as :

$$\Gamma(c) = c\frac{D}{d^2}4\pi r^{*2}d \tag{4.6}$$

One has to choose a physically reasonable value for d. Dee takes about twice the molecular size of a precipitate particle. The nucleation and growth rate is then given by the product of the number of critical nuclei $N_{critical}$ times the rate at which they grow, $\Gamma(c)$. $N_{critical}$ is given by (4.1), where the energy barrier to overcome is $E(r^*)$ given by (4.3) and the critical radius is related to the local concentration (i.e., supersaturation) by (4.5). We can thus express $N_{critical}$ as a function of the concentration, $N_{critical}(c)$. We thus finally have for the nucleation and growth rate $J(c) = \Gamma(c)N_{critical}(c)$.

4.2.3 Application to LP

$J(c)$ can be (almost) readily implemented as a non-linear sink term in the nucleation and growth equations presented in Chap.2. The pattern obtained accounts for all the generic laws of LPs in a very physical picture ([5]).

4.3 Spinodal decomposition

Decay from an unstable state (see Fig.(4.1)) follows through spinodal decomposition. It can be seen as the limiting case where all the nucleation activation energy barriers tend to 0. How one describes the dynamics of a system undergoing spinodal decomposition is the object of this section.

4.3.1 Model B

The approach we will present here is a phenomenological one : it relies on the classical delimitation that the mean field free energy $f(\rho)$ is concave inside the spinodal region and convex outside of it. We know a function which has these properties, it is the Ginzburg Landau free energy :

$$F_{GL}(\rho) = -(1/2)\epsilon\rho^2 + 1/4\gamma\rho^4 \tag{4.7}$$

where ρ is an order parameter characteristic of the phase, i.e. magnetization for ferromagnets or concentration of the precipitate in our case. ϵ and γ are temperature-dependent parameters, which are both positive for $T < T_c$. We can use $F_{GL}(\rho)$ to describe phase transitions between the two states which minimize it, $\rho_{l,h} = \pm\sqrt{\frac{\epsilon}{\gamma}}$. We will always take $\epsilon = \gamma$ in the following so that $\rho_{l,h} = \pm 1$, but one should keep that they should be treated in all generality as free parameters.

Remark : of course if ρ is to represent a concentration, it should always be positive. If the two equilibrium states of the free energy are given by $\rho_l > 0$ and $\rho_h > 0$, the order parameter intervening in the model should be $\tilde{\rho} = 2\frac{\rho-\rho_h}{\rho_l-\rho_h} - 1$. Moreover, we dismissed cubic terms in the free energy, which bring about an asymmetry in the double-well potential. This is justified in the case of ferromagnets where the spin-up and spin-down phases are symmetrical. In describing the transition between a dilute and a precipitate phase, we do no longer have such a symmetry. We feel that taking it into account this asymmetry would only complicate the picture without bringing any substantial modifications.

So far, ρ represented a global thermodynamic variable. How do we move on to a description involving a local dynamic concentration $\rho(x,t)$? We proceed by dividing the system in finer cells of dimensions l^3, see Fig.(4.4). The cells are assumed fine enough so that x_α can be considered as a continuous variable x.

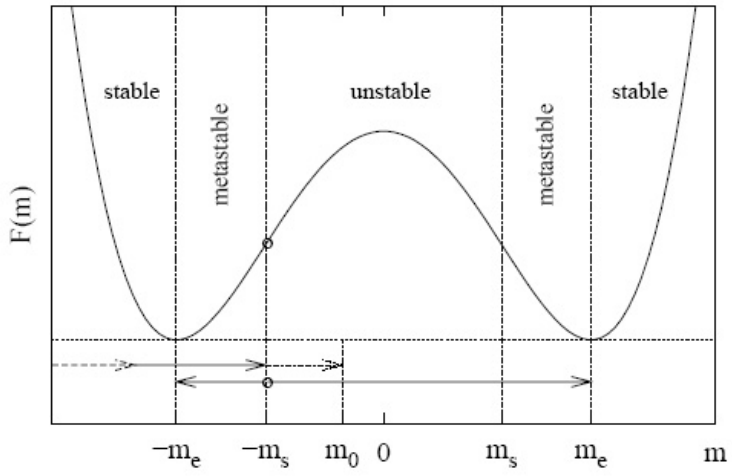

Figure 4.3: A plot of the homogenenous part of the free energy density F_{GL} indicating also the corresponding metastable/unstable regions. Cubic terms in the free energy were dismissed so that the double-well is symmetric.

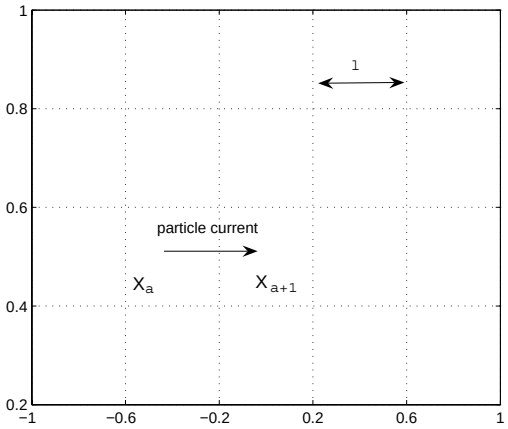

Figure 4.4: Schematic view of the the coarse graining of the physical system.

But on the other hand, they must also be big enough so that a thermodynamic description of them is still plausible : we namely want to extend the free energy (4.7) to each cell, i.e. $F(\rho) \rightarrow F(\rho(x))$. Interaction between the cells will be accounted through a term of the form $\frac{\sigma}{2} \mid \nabla\rho(x) \mid^2$, which describes surface tension between cells of different composition (ie phases). We then obtain a free energy density :

$$f_{GL}(\rho(x)) = 1/2\epsilon\rho(x)^2 - 1/4\gamma\rho(x)^4 + \frac{\sigma}{2}|\nabla\rho(x)|^2 \tag{4.8}$$

and the total free energy of the system for the configuration $\rho(x)$ is given by the integral

$$F_{GL}[\rho(x)] = \int dx \left(1/2\epsilon\rho(x)^2 - 1/4\gamma\rho(x)^4 + \frac{\sigma}{2}|\nabla\rho(x)|^2\right) \tag{4.9}$$

We have not yet used the fact that the density ρ is conserved. It implies

$$\partial_t\rho = -\nabla\vec{j} \tag{4.10}$$

The current of particles is driven by a gradient of chemical potential $\vec{j} = \nabla\mu$. This one can be obtained as a generalization of the thermodynamic relation $\frac{\partial F}{\partial N} = \mu$ to each of the cells in Fig.(4.4), that is

$$\mu(x,t) = \frac{\delta F_{GL}}{\delta\rho}|_{\rho(x,t)}$$

So that our model takes the form :

$$\partial_t\rho = -\triangle\frac{\delta F_{GL}}{\delta\rho} \tag{4.11}$$

Computing the functional derivative , we finally get the Model B equation :

$$\boxed{\frac{\partial\rho(x,t)}{\partial t} = \Delta(-\epsilon\rho + \gamma\rho^3 - \sigma\Delta\rho)} \tag{4.12}$$

Since this equation is a cornerstone for our further developments, it deserves a few comments :

1. It is a fourth-order non-linear PDE and thus doesn't lend itself well to analytical calculations. Existence and uniqueness of solutions of the model have however been demonstrated. The first term is diffusive, but with a "negative diffusion coefficient" (since $\epsilon > 0$). The fourth order term is mathematically indispensable to make this equation a regular one (no blow ups).

2. The *spinodal* is given by the condition

$$\frac{\partial^2 f(\rho)}{\partial \rho^2}|_{\rho_s} = 0 \quad \leftrightarrow \rho_s = \pm\sqrt{\frac{\epsilon}{3\gamma}}$$

3. Linear stability analysis can give us insight in the behaviour of (4.12). Let's consider a small perturbation around a homogeneous concentration, $\rho = \rho_0 + \delta\rho$. Keeping only the linear terms in $\delta\rho$ gives :

$$\delta\dot{\rho} = \triangle(\epsilon\delta\rho - 3\gamma\rho_0^2\delta\rho + \sigma\triangle\delta\rho) \tag{4.13}$$

Making a spatial Fourier transform, we get :

$$\delta\dot{\rho}(k,t) = \delta\rho(k,t)\left(k^2(3\gamma\rho_0^2 - \epsilon) - \sigma k^4\right) \tag{4.14}$$

The right hand side is always negative if $|\rho_0| > |\rho_s|$, ρ_0 is thus a stable solution in this domain. On the other hand, when $|\rho_0| < |\rho_s|$, those modes for which $|k|^2 < \frac{3\gamma\rho_0^2 - \epsilon}{\sigma}$ become unstable. We have what is called a *long wave-length instability* of the model. Typically, a composition fluctuation in the form of a δ-function will contain in its spectrum all the wavelengths and will thus be able to trigger the instability if $|\rho_0| < |\rho_s|$.

4. Model B is very similar to the Ginzburg-Landau description of superconductors. In particular, it has the same kink-solution (linking the two stable states) as in the theory of superconductivity :

$$\rho_{kink}(x) = \tanh(\frac{x}{\xi}) \quad \text{with} \quad \xi = \sqrt{\frac{2\sigma}{\epsilon}} \tag{4.15}$$

ξ gives the thickness of a typical interface.

5. Fig.(4.6) gives a typical example of the evolution of a system undergoing spinodal decomposition as described by Eq.(4.12).

4.3.2 Spinodal decomposition as a possible mechanism for LP formation

Model B was originally introduced in the context of phase separation of alloys composed of two species, say iron and carbon, separating into an iron-rich

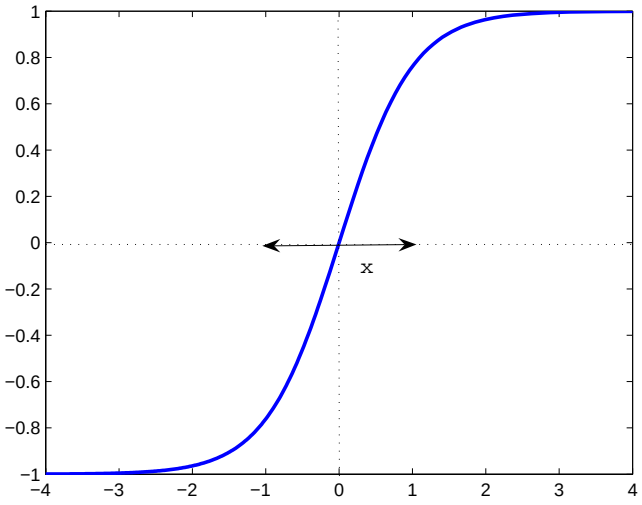

Figure 4.5: Plot of the kink solution (4.15) to Model B, with characteristic interface width $\xi = 1$.

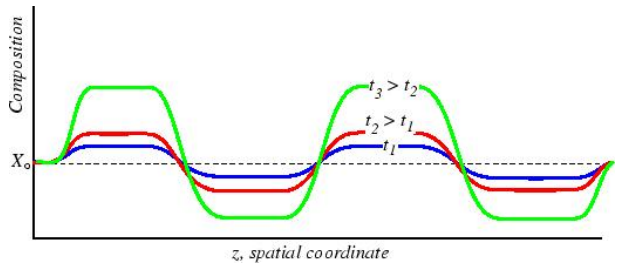

Figure 4.6: Schematic evolution of an unstable density undergoing spinodal decomposition, at three different times

and a carbon-rich phase.

The idea of the scenario developed in [25] is that phase separation in LP formation is not driven by nucleation but by spinodal decomposition. The main fact supporting this view is that homogeneous nucleation times can be dreadfully long, whereas ring formation is observed to take place on a relatively short time scale. If the system doesn't contain any impurities, the only way to cope with this experimental observation would be to invoke spinodal decomposition. So what do experiments say ?

First of all, that impurities do play an important role. P. Hantz[2] reported comparisons between Liesegang experiments in extremely clean and normal environments. It turned out that - all other parameters being held constant - rings didn't even appear if the dishes were clean ! One may argue that the concentration deposited by the front in this case didn't hit the spinodal. There is unfortunately no experimental evidence (and no easy way to prove the fact) that spinodal decomposition is at play and not nucleation. And even that spinodal decomposition ever occurs in gels. In fact, Model B was never used so far to describe precipitation, and therein may well lye its merit and glory.

Not knowing which of the two mechanisms is at play, the ideal would be to be able to write both in the frame of one single equation. This is what we will carry out in the next section.

4.4 Adding noise

4.4.1 The Cahn-Hilliard-Cook equation

The problem of Model B is that a metastable uniform concentration will indefinitely stay as such. The idea of Cook was thus to add a gaussian white noise :

$$\dot{\rho}(x,t) = \triangle\left(\varepsilon\rho - \gamma\rho^3 + \sigma\Delta\rho\right) + \nabla\xi(x,t) \tag{4.16}$$

$$\langle\xi(x,t)\rangle = 0 \qquad \langle\xi_\mu(x,t)\xi_\nu(x',t')\rangle = 2D\delta(t-t')\delta(x-x')\delta_{\mu\nu} \tag{4.17}$$

ξ is a vector noise with three components ξ_μ. The ∇ in front of ξ ensures the conservation of the total density. By including these fluctuations, the spinodal line becomes a spinodal transition zone of typical width $\langle\xi(x,t)^2\rangle$.

[2]Private communications.

Now, in a metastable state, fluctuations may at any time (and with greater probability the closer to the spinodal) provoke a local crossing of the spinodal and thus trigger phase separation. Can we then say that, through the addition of this noise term, we capture both the spinodal *and* the nucleation regime ? But where then do the notion of a critical radius and nucleation rate come into play ?

The critical nucleation radius in Model B

Let's consider the following two states : "1" consists of a uniform metastable density $\rho_0 < -\rho_s$ over a length L, while "2" is the same state, but with a segment of it (a droplet) which we promoted to $\rho_h = +1$ over a length Δx.

Let's compute for each of them the total free energy. For "1" it is just (taking $\epsilon = \gamma$) :

$$F_1 = (-\frac{1}{2}\epsilon\rho_0^2 + \frac{1}{4}\epsilon\rho_0^4)L$$

For 2 , it is, if we take E_i to be the energy of an interface and E_{min} the energy of the ± 1 phase

$$F_2 = (-\frac{1}{2}\epsilon\rho_0^2 + \frac{1}{4}\epsilon\rho_0^4)(L - \Delta x) + \Delta x E_{min} + 2E_i$$

E_i can be estimated by integrating the surface tension term $1/2\sigma(\partial_x\rho_{kink})^2$ where ρ_{kink} is the kink solution (4.15) presented earlier. We get $E_i = 0.614\frac{\sigma}{\xi} \sim \frac{\sigma}{\xi}$. E_{min} is $-\frac{1}{4}\epsilon$. The critical radius Δx_c is then given by the condition $F_1 = F_2$.

$$\Delta x_c = \frac{\xi}{1/4 - (\rho_0^2/2 - \rho_0^4/4)} \tag{4.18}$$

We tested this relation numerically by measuring systematically the size of the critical nucleus under different metastable concentrations. The method used was to abruptly push the concentration to $+1$ over a distance r and see whether the thus created droplet was stable over a given observation time. Starting at very high radius, we gradually decrease it until the droplet is seen to be swallowed by its surroundings. This point was identified with the critical droplet size. Fig.(4.7) shows the results obtained while Fig.(4.8) illustrates the evolution of super- and sub-critical droplets.

It seems that the theoretical relationship (4.18) has little to do with the curve obtained. The critical radius gets smaller as the supersaturation grows, which is correct. Its precise dependance may however not be in agreement

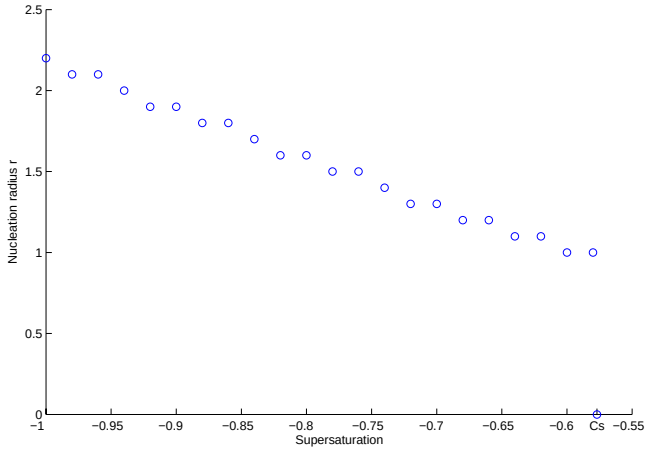

Figure 4.7: Measurement of the critical nucleation radius as a function of supersaturation for Model B, $\epsilon = \gamma = \sigma = 1$. The homogeneous metastable concentration was perturbed by an increase to $\rho_h = +1$ over a given radius. On the time of observation of the simulation, the radius was not found to blow up at $\rho_0 = -1$ as it should; this is due to the very slow absorption of large droplets. The radius should also go to 0 at ρ_s, since any perturbation induces spinodal decomposition at this value : once again, our observation time was too short to observe this behaviour.

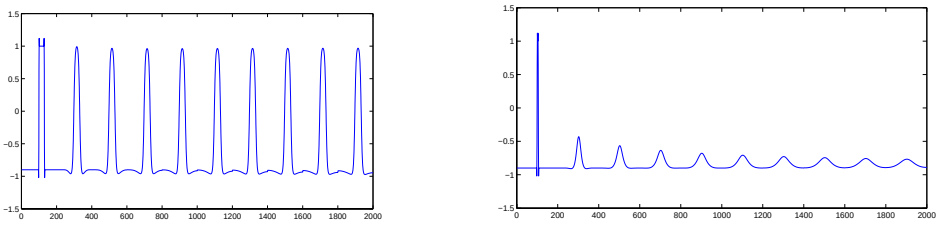

Figure 4.8: Evolution of super- and sub-critical droplets in Model B, $\epsilon = \gamma = \sigma = 1$.

with the prediction of nucleation theory, as obtained in (4.5).

The main conclusion is that the critical nucleus behaviour as observed in Model B is a slowly varying and decreasing function of the supersaturation, just as (4.5).

Nucleation rate in Model B with noise

How does the exponential dependance (4.1) appear in Model B' ? The number of super-critical droplets should be proportional to the concentration times the probability that a fluctuation exceeds the spinodal threshold. If the initial metastable concentration is c_0, this probability is given by

$$\int_{c_s-c_0}^{+\infty} d\xi \frac{1}{\sigma\sqrt{2\pi}} e^{-\xi^2/(2\sigma^2)} \propto \mathrm{erfc}\,(c_s - c_0/\sigma) \tag{4.19}$$

where as we will see the variance is $\sigma^2 \propto k_B T$. Now the erfc function could be expanded in the limit of small initial supersaturations, $c_0 \ll c_s$, giving an exponential term

$$\mathrm{erfc}\,((c_s - c_0)/\sigma) \approx e^{-\left(\frac{(c_s-c_0)}{\sigma}\right)^2} \frac{\sigma}{\sqrt{\pi}(c_s - c_0)} \tag{4.20}$$

So we recover, not very rigorously we conceed, the exponential term in the number of droplets (4.1), with some prefactors[3].

Growth in Model B with noise

Notice that in the picture of the transition from a metastable state to equilibrium presented above, the dynamics is still described by spinodal decomposition, though it is the fluctuations which are responsible for its taking off. It is unclear in how far this is justified and links with the physical picture of growth involving surface aggregation as is incarnated by (4.6). Our equation seems to rely too heavily on the GL form of the free energy (which after all is the simplest double-well potential) to include this feature as well. We shall however disregard this fact as not being of capital importance for a qualitative explanation of LPs.

[3]This last calculation would require more careful examination. In fact the obtained result doesn't depend on the droplet size contrary to (4.1). It is not clear whether taking into account this dependence would only add prefactors or possibly modify the functional form of (4.20)

A problem with the Cahn-Hilliard-Cook equation

We now have an equation (4.16) which should - in principle - describe the whole range of possible precipitation behaviours. But the noise term is actually flawed if we think of the ρ of (4.16) as a concentration $c(x,t)$: it permits local density fluctuation of C's independently of whether yes or no there is any C there ! What would be possible in the case of a magnet having local magnetization fluctuations becomes obviously unphysical for a concentration.

So we have to work a bit more : the noise has to somehow be multiplied by the local concentration $c(x,t)$. We know from equilibrium statistical physics that the fluctuations in concentration go as $\sqrt{c}$. A first guess for the noise term would thus be :

$$\nu(x,t) = \nabla(\sqrt{c(x,t)}\xi(x,t)) \tag{4.21}$$

Such a noise which depends on the stochastic variable $c(x,t)$ itself is termed a *multiplicative noise*. There exist two conventions for averaging the quantity $\langle\nu(x,t)\rangle$, which yield different results. They are respectively called the Ito and Stratonovich conventions (more detail can be found in Appendix A) :

- Ito says :

$$\langle\nu(x,t)\rangle = 0$$

- Stratonovich says :

$$\langle\nu(x,t)\rangle = \frac{T\Delta t}{2}\nabla\left(\frac{\nabla c}{c}\right)$$

Ito and Stratonovich calculus yield the same result if the stochastic term is additive (as in the usual Langevin equation), and in this case there is no ambiguity.

In order to know which of the two conventions one should use, one could ideally start from a microscopic description with additive noise (but this is unfortunately very often a difficult task). One can then carry on the calculation in either of the two conventions, the results will be the same for the averages and the correlation functions (ie the physical quantities of interest).

In the case of (4.21), in order to know which of the two conventions is the correct one, one has to come back to a more physical equation containing only additive noise. This will be done in the following section.

4.4.2 Model B' : a density functional theory

We follow in this section Dean's reasoning, [16]. A good (unambiguous) equation to start from in order to include fluctuations is the Langevin equation for the position X_i of the i-th particle, $i = 1 \dots N$. Its deterministic part should include interactions with the other particles which can give rise (for a large number N of particles) to the existence of separate phases. Our starting point will thus be

$$m\ddot{X}_i = \sum_{j=1}^{N} V(\mid X_i - X_j \mid) - \kappa \dot{X}_i + \xi_i \qquad i = 1 \dots N$$

κ is the viscosity. Since we are not interested in the regime where strange initial velocity conditions might play a role, and we suppose the viscosity of the media (a gel in our case) high enough for those to fade away quickly, we will immediately consider the *over-damped* regime in which the acceleration of the particles can be neglected compared to their velocities, so

$$\dot{X}_i(t) = \frac{1}{\kappa}\xi_i(t) - \frac{1}{\kappa}\sum_{j=1}^{N} \nabla V(X_i(t) - X_j(t)) \tag{4.22}$$

The correlation function of the noise is given to us by the requirement that the velocity-distribution function be a Maxwellian (equilibrium) one at long times. This requirement is also called a fluctuation-dissipation theorem and yields, if we absorb $1/\kappa$ in the noise :

$$\langle \xi_i(t)\xi_j(t) \rangle = \frac{2k_B T}{\kappa}\delta_{ij}\delta(t - t') = 2D\delta_{ij}\delta(t - t') \tag{4.23}$$

We identified the quantity $\frac{k_B T}{\kappa}$ with the diffusion coefficient D, since it is the one appearing in front of the diffusion term if we compute the Fokker-Planck equation associated to (4.22). The dependance of D on the mass of the brownian particles ($D \propto 1/m$) is comprised in κ.

We want an equation for the density defined as

$$\rho(x,t) = \sum_{i=1}^{N} \delta(X_i(t) - x) = \sum_{i=1}^{N} \rho_i(x,t)$$

A change of variable for a stochastic differential equation (SDE) necessitates the choice of either one of the Stratonovich or Ito convention. We will choose the Ito one here, relegating the Stratonovich derivation and more calculation details to Appendix B, since it provides a nice illustration of the dilemna we just mentioned. Of course both lead to the same result. Using Ito formula for a change of variable, integration by parts, summing over all the particles, and absorbing $1/\kappa$ in the interaction potential, we get (see Appendix B for more details) :

$$\frac{\partial \rho}{\partial t} = \underbrace{-\sum_{i=1}^{N} \nabla(\xi_i \rho_i(x,t))}_{Noise} + \underbrace{\nabla(\rho(x,t) \int dy \rho(y,t) \nabla V(x-y)) + T\nabla^2 \rho(x,t)}_{Deterministic \quad part} \tag{4.24}$$

Simplification of the noise term

The noise term contained in (4.24) contains too much information about the individual particles. We wish to transform it to an equivalent noise term involving the total density $\rho(x,t)$. If we define

$$\nu(x,t) = \sum_{i=1}^{N} \nabla(\xi_i \rho_i(x,t)) \tag{4.25}$$

then

$$\langle \nu(x,t)\nu(x',t') \rangle = 2D\delta(t-t') \sum_{i=1}^{N} \nabla_x \nabla_{x'} (\rho_i(x,t)\rho_i(x',t)) \tag{4.26}$$

By using the following property of the δ-function which basically states that no particle can be in two places at the same time,

$$\rho_i(x,t)\rho_i(x',t) = \delta(x-x')\rho_i(x,t) = \delta(x-x')\rho_i(x',t) \tag{4.27}$$

We find

$$\langle \nu(x,t)\nu(x',t') \rangle = 2D\delta(t-t') \sum_{i=1}^{N} \nabla_x \nabla_{x'} (\delta(x-x')\rho(x,t)) \tag{4.28}$$

But the Gaussian noise field defined as

$$\nu'(x,t) = \nabla(\xi(x,t)\sqrt{\rho(x,t)}) \tag{4.29}$$

has exactly the same correlation function and can therefore replace $\nu(x,t)$ in (4.24).

We have rigorously derived the noise term predicted in the last section. It is to be averaged in the Ito sense, since that is the convention we chose from the start, that is

$$\langle \nu'(x,t) \rangle = 0 \tag{4.30}$$

so there is no systematic noise contribution to the dynamics of $\langle \rho(x,t) \rangle$.

Remark : the density used so far is defined as a sum of delta functions. At some point it should undergo a spatial coarse-graining procedure in order to obtain a smooth density $\rho_{\substack{coarse \\ grained}}(x,t)$ which we can differentiate in the usual way. In the following, we will thus consider that we are working with a density defined as

$$\rho_{\substack{coarse \\ grained}}(x,t) = \frac{1}{V}\int_V dx \rho(x,t)$$

where V is a small coarse graining volume so that $\rho_{\substack{coarse \\ grained}}(x,t)$ is smooth. We will however continue to denote the density $\rho(x,t)$ in order not to overload the notations.

Rewriting the deterministic part as a function of the free energy

The free-energy of the system can be written as

$$F = \underbrace{\frac{1}{2}\int dxdy\rho(x)V(x-y)\rho(y)}_{Potential \quad Energy} + \underbrace{D\int dx\rho(x)log\rho(x)}_{Entropy} \tag{4.31}$$

where kinetic-energy terms were omitted since the overdamped regime is equivalent to having particles of zero mass (no inertia). (4.24) can then be rewritten

$$\frac{\partial \rho}{\partial t} = \nabla\left(\rho\nabla\frac{\delta F}{\delta \rho}\right) + \nabla\left(\xi(x,t)\sqrt{\rho(x,t)}\right) \tag{4.32}$$

Now the assumption we make to fall back on a Model B type equation is to identify the free energy F with the Ginzburg-Landau one. One of course

wonders if there wouldn't be a rigorous coarse-graining procedure that would get us from the free energy naturally given as in (4.31) to the GL form for a given interaction potential of the particles (for instance the Lennard-Jones one). This is a general statistical physics question which we didn't investigate in the course of this work. An attractive feature of the present derivation is that the free energy appeared without any approximation or coarse graining (in contrast to the derivation of Model B presented above).

If the two equilibrium states of the free energy are given by ρ_l and ρ_h, the order parameter intervening in the model is $\tilde{\rho} = 2\frac{\rho-\rho_h}{\rho_l-\rho_h} - 1$, Model B' finally writes

$$\boxed{\frac{\partial \rho}{\partial t} = \nabla \left(\rho \nabla \left(\varepsilon \tilde{\rho} - \gamma \tilde{\rho}^3 + \sigma \triangle \tilde{\rho} \right) \right) + \nabla \left(\xi(x,t) \sqrt{\rho(x,t)} \right)} \tag{4.33}$$

Notice that the deterministic part has changed in comparison to (4.12). The $\triangle$ operator in front of $\frac{\delta F}{\delta \rho}$ has become a $\nabla \rho \nabla$. This change would have been completely overseen had we just proceeded to the addition of the noise (4.21) to Model B. This is a vivid illustration of an article by Van Kampen ([7]) relating the debacles of physicists trying to add "by hand" multiplicative noise terms.

One can compute the Fokker-Planck equation associated to (4.33) and verify that the probability distribution of the configurations $P_{st}[\rho] \sim \exp(\frac{-F[\rho]}{kT})$ is a steady state solution. The fluctuation-dissipation theorem is thus satisfied by Model B'. Model B with a simple additive noise term also satisfies the fluctuation-dissipation relation, but putting a multiplicative noise spoils this property. Model B' provides a remedy to this by changing the deterministic part.

If in the free energy, we put the interactions to zero and keep only the entropic term, we recover the diffusion equation, which is what one definitely expects from a gaz of brownian particles.

Equation (4.33) was interestingly also derived in [14] on different grounds : they proceeded by supposing a concentration dependent rate in the master equation for the composition of the cells $\rho(x_\alpha)$. Following the line of thought of Langer [8], they end up with a generalized version of Model B involving a concentration dependent diffusion coefficient. If we choose the latter of the form $D(\rho) \propto \rho$, we end up with (4.33).

Phenomenological derivation

Equation (4.33) can also be derived on phenomenological grounds in the spirit of what we presented for Model B. Invoking the local conservation of the density and a current $\vec{j}$ given by :

$$\begin{aligned} \frac{\partial \rho}{\partial t} &= -\nabla \vec{j} \\ \vec{j} &= -\rho \nabla \frac{\delta F}{\delta \rho} \end{aligned} \tag{4.34}$$

we arrive to (4.33), without the noise of course. Actually, this form of the current makes more sense than just $\nabla \frac{\delta F}{\delta \rho}$ since it involves a given density being dragged by the force $\nabla \frac{\delta F}{\delta \rho}$, just as, for instance, an electric current is given by the local density of charge times its velocity $\vec{j}_{electric} = \rho \vec{v}$.

Discussion of the noise term

Notice that the noise (4.23) is taken to act independently on each particle. This hypothesis will strongly limit the domain of validity of our resulting equation. In fact, let us imagine that the precipitate appearing in Liesegang pattern is a perfect crystal where atoms are bound to each other by spring-like forces. We know that each *collective* mode of this crystal will have a typical occupation number due to thermal fluctuations. Supposing the noise term of each site in the crystal independent of the others would be courting disaster. This is of course an over-idealization of what the real precipitate looks like, but it nevertheless warns us that we shouldn't expect the noise-term to hold in the precipitate phase.

An interesting feature of fluctuations is the dynamical equilibrium of the reaction $A+B \leftrightharpoons C$ at the interface of a precipitate band, that is the possible re-dissolution of the solid state C. Such an effect was observed in several experiments where bands appeared to "move" due to their dissolution on one side and re-precipitation on the other. This unfortunately goes beyond the scope of this thesis.

4.5 Conclusions

We presented the major mechanisms that are believed to be at play during precipitation. A physically founded extension of Model B, which now

includes fluctuations and thus the whole range of first order phase transitions, has been derived. In the course of this modification, the deterministic part has also changed, in agreement with the fluctuation-dissipation theorem requirements.

Chapter 5

Liesegang patterns: a phase transition scenario

All the necessary physical processes happening in our Petri dish have been gathered; we know how the C gets deposited in the system and we know how this C can aggregate. The assumption we now make it that these two processes are independent : the feedback of the aggregation on the reaction speed can be considered as negligible. This fact is supported by the experimental verifications of the time-law: the reaction front seems to go on diffusively independently of the transformations taking place behind it. At worst, its diffusion coefficient D_f might be replaced by an effective one $\tilde{D}_f$. So we write :

$$\frac{\partial \rho}{\partial t} = \nabla \left(\rho \nabla \left(\varepsilon \tilde{\rho} - \gamma \tilde{\rho}^3 + \sigma \triangle \tilde{\rho} \right) \right) + S(x,t) + \nabla \left(\xi(x,t) \sqrt{\rho(x,t)} \right) \tag{5.1}$$

where

$$S(x,t) = \frac{A}{t^{2/3}} \exp \left(- \frac{(x - x_f(t))^2}{2w(t)^2} \right) \tag{5.2}$$

as was derived in (3.13) and the characteristics of the noise are

$$\langle \xi(x,t) \rangle = 0 \qquad \langle \xi_(x,t) \xi_(x',t') \rangle = 2D\delta(t-t')\delta(x-x') \tag{5.3}$$

Note that the only free parameters are :

- σ for Model B' since ε can be absorbed in the definition of time, and $\varepsilon = \gamma$ in order to have the right equilibrium states.
- a_0, b_0, k and D for the source, which are expressed through D_f, w_0 and A in (3.13). One of them disappeared in the course of this listing due to the dependence of the initial problem just on the ratio a_0/b_0.

5.1 The noiseless limit

5.1.1 Reproducing Liesegang banding

Let us warn the reader that most of the results presented in this section are contained in Ref.[25] for Model B. Since the deterministic part in (5.1) changed, we must make sure that the "old" features of Model B can be recovered.

The mechanism

The mechanism for the formation of bands is the same as was sketched in Chap.2, where the role of the threshold is played by the spinodal c_s. The depletion effect is due to the "draught" of C's necessary to reach the equilibrium concentration $c_h = +1$ while conserving the overall quantity of C. The source moves on until it reaches again the spinodal, leading to a second band etc.

Results

Fig.(5.1) gives a typical simulation result of equation (5.1) without noise.

Banding is clearly observed. In order to verify whether the spacing law is satisfied, the positions of the bands x_n were very nicely fitted by two-parameter functions of the form $x_n = Q(\exp(\tilde{p}n) - 1)$. Thus the model contains the spacing law with the spacing coefficient given by $1+p = \exp(\tilde{p})$.

Next, one can investigate whether the patterns in our model obeys the Matalon-Packter law. What we did in order to verify this is to freeze the concentration b_0 and vary between different values of a_0 in order to reveal the $1/a_0$ dependence in (1.3). Of course we have to translate these values of a_0 and b_0 in terms of the relevant parameters of $S(x,t)$, w_0, D_f and A. Results are shown in Fig.(5.2); they show very good agreement with the Matalon-Packter law.

Let us finally mention that the width of the front is found to have very little effect on the resulting pattern : whenever more handy, we in fact used the approximation of infinite reaction rate.

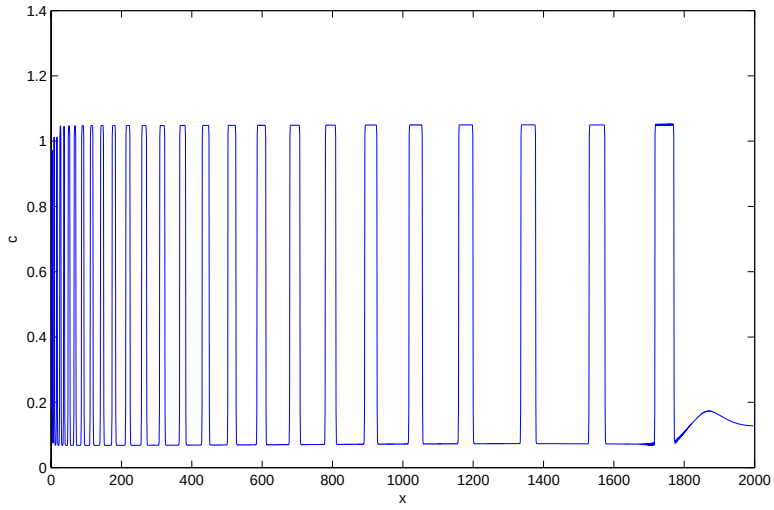

Figure 5.1: Concentration profile obtained for the following values of the front parameters: $D_f = 21.72$, $w_0 = 4.54$, and $A = 0.10$, $\epsilon = \gamma = 10$ and $\sigma = 1$.

Choosing the parameters

Typical experimental situations correspond to concentrations a_0 and b_0 of the reagents of the order of $10^{-2} - 10$ M, with a ratio $a_0/b_0 \sim 10 - 100$, and thus it is suitable to choose the unit of concentration as $n_0 = 1$ M. The diffusion coefficients of the reagents are of the order $\sim 10^{-9}$ m^2/s, so that the length ℓ and time τ scales should be chosen such that ℓ^2/τ is of the same order of magnitude,

$$\frac{\ell^2}{\tau} \sim D\,.$$

Moreover, the experimental patterns have a total length of about 20 cm, and the time to produce such a pattern is of some tenth days – and this offers the order of magnitude of the diffusion coefficient of the reaction front, which is typically of the same order or an order of magnitude larger than the diffusion coefficients of the reagents (depending on the ratio a_0/b_0 of the concentration of the reagents). The typical widths of the precipitation bands are of a few mm at the beginning, and approach ~ 1 cm at the end, and so are the distances between two successive bands. From the visual observation of the beginning of the band formation it takes some tenth minutes for the band to be clearly seen, and some hundred minutes for its complete formation.

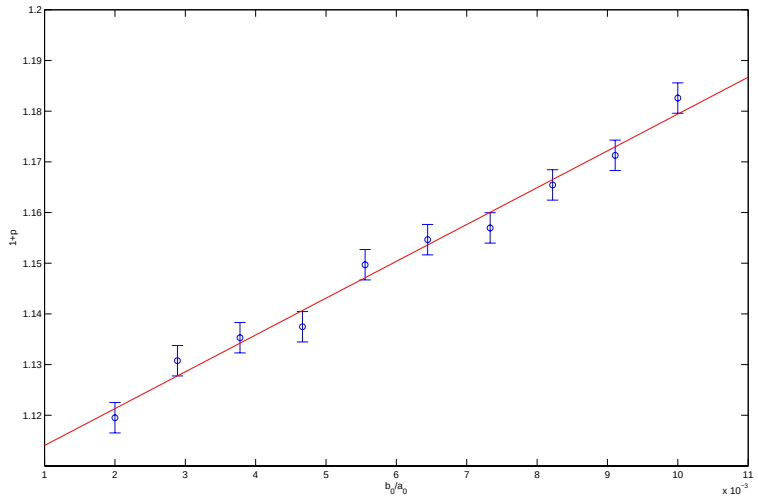

Figure 5.2: Variation of the spacing parameter p as a function of b_0/a_0 for a fixed $b_0 = 0.12$ M. The trend can be well approximated by a linear one, thus confirming the Matalon-Packter law. The abscise and slope of this curve give us respectively one point of the functions $F(b_0)$ and $G(b_0)$ intervening in (1.3).

Since the Cahn-Hilliard model has intrinsic length scale $\sqrt{\sigma/\varepsilon}$ and time scale $\sigma/(\lambda\varepsilon^2)$, these have to be comparable to the typical length and time scales of the appearance of a single band. We are thus led to the following orders of magnitude for the length and time scales:

$$\ell = \sqrt{\sigma/\varepsilon} \sim 10^{-4}\,\mathrm{m}\,, \quad \tau = \sigma/(\lambda\varepsilon^2) \sim 10\,\mathrm{s}\,.$$

Concerning the concentrations c_l and c_h, they could be measured from experiment, but since that has not yet been done, we choose one of them (the other being then given by the corresponding point on the coexistence curve) such that c_0 lies in in the instability domain. This approach would in fact gain credit if these concentrations were to be measured.

5.1.2 Equidistant patterning

One of the most interesting features of Model B' (and Model B), which also lends itself well to analytical calculations, appears in the case where the reaction-diffusion front moves much faster than it takes time for the spinodal instability to set in, see Fig.(5.3). This behaviour can be reached by setting the effective diffusion coefficient to high values compared to the kinetics of the precipitate aggregation. Striking in the above picture are:

- The well definite wave-length λ of the pattern. The bands appear equidistantly and not in a geometric progression. This regime doesn't however last forever: running the simulations for a longer time shows that we inevitably come to a point where the instability catches up the reaction front. The usual spacing law behaviour then sets in.

- The well definite speed v of the propagation of this instability, which seems to be constant. Since the front travels with a $\sqrt{t}$ law, it is obvious that the instability will eventually reach the reaction front.

As can be seen from Fig.(5.3), in this regime, the front and the instability are widely separated spatially. One can thus consider an idealized version of the problem where an initially homogeneous, unstable ($c_0 > c_s$) concentration is perturbed by, say, a δ-function kick.

Mathematical guesses

For the simplicity of the calculation, we will consider Model B as defined in (4.12), but the reasoning can be equally well applied to (4.33).

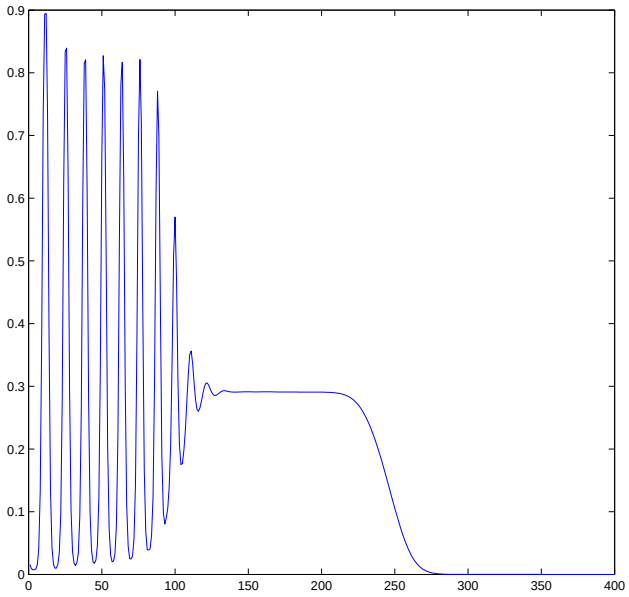

Figure 5.3: Equidistant patterning obtained by a front moving much faster than the instability sets in. Parameters are : $D_f = 80$, $A = 0.2$ and $\epsilon = \gamma = 1$
.

The speed and the wavelength must somehow be related to the coefficients ϵ, σ appearing in (4.12), and to the unstable concentration c_0. A first hint is given to us by dimensional analysis : the only two quantities which have the dimensions length and speed are

$$\begin{aligned} v &\propto \epsilon^{1/2}\sigma^{1/2} f(c_0^3) \\ \lambda &\propto \frac{\sigma}{\epsilon} g(c_0^{-1}) \end{aligned} \tag{5.4}$$

where the function f and g are functions that don't change the power of their argument. We know that for $|c_0| \geq c_s$, no instability occurs. A good guess for g and f would thus be $g(c_0) = f(c_0) = \sqrt{3c_0^2 - 1}$, since it yields in the limit $c_0 \to c_s$ that no wave takes place, ie, $v \to 0$ and $\lambda \to \infty$. We will now try to find the constant of proportionality in these relations.

The behaviour of (4.12) a short time after the perturbation is given by the linear stability analysis around c_0. We reproduce here the calculation performed in Chap.4, setting $\epsilon = \sigma = 1$:

$$\delta\dot{c}(k,t) = \delta c(k,t)\left(k^2(3c_0^2 - 1) - k^4\right) \tag{5.5}$$

A first, albeit not rigorous, argument is the following : the function at the left hand side has a maximum at $|k_{max}| = \sqrt{\frac{3c_0^2-1}{2}}$ and thus theses modes will be the fastest growing ones. One can also expect that they will be the ones "deciding" of the wavelength of the pattern once frozen. This gives a first (and good as will be seen) approximation of λ.

In order to compute the speed, one could try to input a travelling wave solution $c(x,t) = c(x - vt) \equiv c(\eta)$ in (4.12). We get the following equation for v:

$$-vc' = -(c'' - (c^3)'' + c'''') \tag{5.6}$$

Unfortunately, (5.6) doesn't have any simple solutions, and a phase plane analysis doesn't provide any insight into possible restrictions on v[1].

[1] A phase plane analysis consists in putting the equation in the "mechanical" form $\ddot{c} = -v\dot{c} + \frac{d}{dc}[f(c)]$ and seeing what would be the possible trajectories with the potential $f(c)$.

Rigorous calculation

I am indebted to Z.Racz for the results of this paragraph. In Fig.(5.3), one sees well that it is the tail of the instability which "drags" it forward, and that in this region, the linear behaviour 5.5 is valid. We will thus concentrate on this region. The solution of (5.5) being of the exponential form, we have, switching back to real space and denoting $a = (3c_0^2 - 1)$,

$$\delta c(x', t) = \int e^{-ikx'} e^{t(ak^2 - k^4)} dk \tag{5.7}$$

which is only valid for $x' \approx vt$, so:

$$\delta c(x', t) = \int e^{\left(k^2(a-k^2) - ikv\right)t} dk \equiv \int e^{-\omega(k)t} dk \tag{5.8}$$

The behaviour of this integral can be evaluated by the saddle point method[2]. Moreover we must impose that at the saddle point k^*, the argument of the exponential be purely imaginary so that we end up with an oscillatory integral, and not an exponentially growing one. We thus have the conditions :

$$\begin{aligned} \left.\frac{\partial \omega}{\partial k}\right|_{k^*} &= 0 \\ \mathrm{Re}(\omega(k^*)) &= 0 \end{aligned} \tag{5.9}$$

We can express v as a function of $k^* = \rho e^{i\phi}$ by the second equation. The first equation has three different roots, of which only the two complex conjugated ones are found to be acceptable. They yield (as awful as it may look) :

$$\begin{aligned} v &= \frac{2}{3}\left(\frac{1}{\sqrt{\sqrt{7}+1}} + \sqrt{\sqrt{7}+1}\right) a^{2/3} \\ \mathrm{Im}k^* &= \frac{1}{2}\frac{1}{\sqrt{\sqrt{7}+1}} a^{1/2} \\ \mathrm{Re}k^* &= \frac{1}{2}\frac{\sqrt{\sqrt{7}+3}}{2} a^{1/2} \end{aligned} \tag{5.10}$$

[2]A brief reminder of saddle point method : the dominant contribution in an integral of the type (5.8) comes from the minima $\omega'(k)|_{k^*} = 0$, $\omega''(k)|_{k^*} > 0$. The integral is then $\sqrt{\frac{2\pi}{\omega''(k^*)}} e^{-\omega(k^*)}$.

We thus have the speed and the wave number. What does the imaginary part of k^* describe ? If we take a look at Fig.(5.3), we see that the peaks of density describe an envelope near the point where the instability propagates, just as any damped oscillations do. This damping is exponential and the imaginary part of k^* gives us the coefficient in the exponent.

Coarsening

We want to emphasize that the occurrence of this equidistant patterning regime is only transient : this part of the pattern actually undergoes coarsening after a certain amount of time, leading to band coagulation. The resulting wave length of the pattern at long times is approximately twice the one it was at formation (which we calculated). This is a result of a non-linear effect.

Is this regime experimentally observable ?

Obtaining systematic equidistant patterns would be an important step in the application of Liesegang phenomena as was mentioned in Chap.1. The behaviour observed here above seems to suggest a way of getting such patterns. Let us however contain some of our wishful thinking and remark the following :

- It is not clear whether the situation where the front travels faster than the aggregation takes place actually can happen in real systems. It would probably only occur at the very beginning of the process, where most experiments report a precipitate "plug" due to the convection effects of the liquid outer electrolyte. However taking a look at pictures like Fig.(5.4) sure seems to suggest that something close to this regime can be achieved.

- These first bands may actually be very thin and not be seen by eye examination.

- There can be coarsening leading to the formation of a "plug".

The experiment which provides the best evidence of the reality of this regime was theoretically treated in a similar way by [12] and is not actually what one would call a LE since it deals with a metallic alloy being spread by epitaxy on a substrate. But it certainly illustrates well the theoretical findings presented in this section.

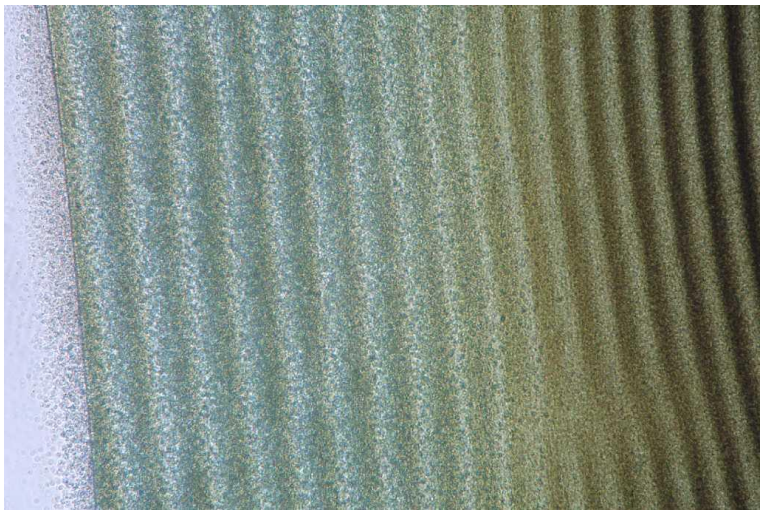

Figure 5.4: Almost equidistant bands obtained in a CuO system, from [32].

5.2 The influence of noise

All the species present in the gel undergo thermal agitation, which is the reason for their diffusion in the gel. So far, the number of studies which included the effect of fluctuations on LP formation is fairly restricted : in [9], the Liesegang phenomena is reproduced by a cellular automata approach. A variety of behaviours, like spiral growth, dendrite formation and irregular patterning are observed. In [30], LP are obtained from what should be the microscopic foundation of model B, a kinetic Ising Model. Spin-up or spin-down regions correspond to the presence or absence of precipitate. The aggregation of the precipitate particles is taken into account by a ferromagnetic spin-exchange (Kawasaki dynamics, conserving the total magnetization) interaction. A hardcore repulsion of the particles is related to the discrete character of the lattice. The source is said to flip the spins (Glauber dynamics) with a given probability. The master equation with these spin dynamics includes all the fluctuations and that is the one that is simulated. Bands are obtained, with somewhat surprising results like the necessity of a third dimension in order to stabilize the pattern in such a model.

Unfortunately, this second approach is very computer-time consuming and does not lend itself well to the exploration of the large parameter window we have at hand. The master equation clearly contains too much information. Its coarse grained version, the Langevin equation embodied in (4.33) should

be easier to compute numerically. This is what we will carry out in this section.

5.2.1 Is noise significant ? Order of magnitude of the correction.

In the preceding section, we saw that the deterministic part of Model B' with a source correctly reproduced all the main experimental features of LP. We however omitted the noise term which gives a contribution of its half-width :

$$\Delta c \sim \sqrt{2D_c}\sqrt{c} \sim 10^{-6}\text{mol.L}^{-1} \tag{5.11}$$

where we have taken $c \sim 0.1\text{mol.L}^{-1}$ (the approximate concentration of the minority species B) and $D_c \sim 10^{-10}\text{m}^2.\text{sec}^{-1}$. This last value is a guess since the diffusion constant of the intermediate species C in it's low density (not precipitate) phase hasn't been measured (and it would be a harsh task to do so). But one can expect it to be slightly smaller than the diffusion constants of the reacting ions ($D_{A,B} \sim 10^{-9}\text{m}^2.\text{sec}^{-1}$).

In view of the above, adding noise can, at first glance, seem a futile task. There are however several reasons for taking it into account :

1. We capture in one single picture both nucleation and spinodal decomposition.

2. We suspect noise of being responsible for important morphological defects in the LP. Irregular banding, blank alleys, spiral formation, and fork bifurcation (anastomose) are among the few which were observed, see Fig.(1.4). We would like to see in how far these defects can be accounted for by the addition of thermal noise.

3. As said above, the Langevin form of Model B/B' makes it much quicker to compute (it involves solving a PDE and adding random numbers) than the master equation underlying Model B ([30]).

5.2.2 One dimensional case

As discussed, typical values of the noise are of the order $\sqrt{2Dc}$. The length- and time-scale we chose or in units of $l = 10^{-4}m$, $\tau = 10s$. In these units, the diffusion coefficients of the ions are $\tilde{D_A} = \tilde{D_B} = 4l^2/\tau$ and the typical concentration of the B's becomes $\tilde{c_B} = 10^{-5}$ mol.L^{-1}. Thus the order of magnitude of the noise in these units is $N_{ampli} = \sqrt{2\tilde{D}\tilde{c}} \approx 0.01$ on a scale

where $c = 0$ is the precipitate free zone and $c = 1$ represents the precipitate. We denoted by N_{ampli} the width of the gaussian noise entering in 5.1, $\langle \xi^2(x,t) \rangle = N^2_{ampli}$. The whole noise term, that is, including the gradient and the $\sqrt{c}$ will be termed ν.

Depending on whether we choose $N_{ampli} \gg 0.01$ or $N_{ampli} \approx 0.01$, we will be speaking about strong or moderate noise. Weaker noise $N_{ampli} \ll 0.01$ doesn't show any visible effect on the pattern formation and will not be further mentioned.

Strong noise : destruction of the pattern

Such high noise values lead to a complete destruction of the pattern, accompanied by troubling numerical incoherences. In fact, the noise routine incorporates cut-offs for fluctuations leading to negative densities. Systematic appeal to these cut-offs for high noise-values leads to an unbalance in the way the C-profile is "reshuffled" which doesn't respect the conservation of the total concentration.

Moderate (theoretical) noise : correction to the spacing law

We thus turn to somewhat lower noise-values. Fig.(5.5) present typical profiles. The following observation can be made :

1. We observe a residual inter-band concentration of about $c \approx 0.05$. This fact is in agreement with experiments which actually did measure inter-band precipitate concentrations of the same order.

2. We observe more and more bands - for equal length and time-of-formation - with increasing noise. As expected, as the noise increases, the pattern becomes denser and less regular.

This second point can easily be understood : the front needs only deposit a concentration in the metastable region close enough to the spinodal line, fluctuations will then provide the necessary concentration leap to trigger the phase separation. "Close enough" is given by the width of the noise in (5.1), $\sqrt{\langle \nu^2 \rangle}$. Negative density fluctuations obviously do not have any effect. The irreversible crossing of the band will thus occur earlier than it would in the absence of fluctuations.

The spacing-law still remains a good indicator for the positions of the bands. In order to quantify the effect of the noise, we plotted in Fig.(5.6) the

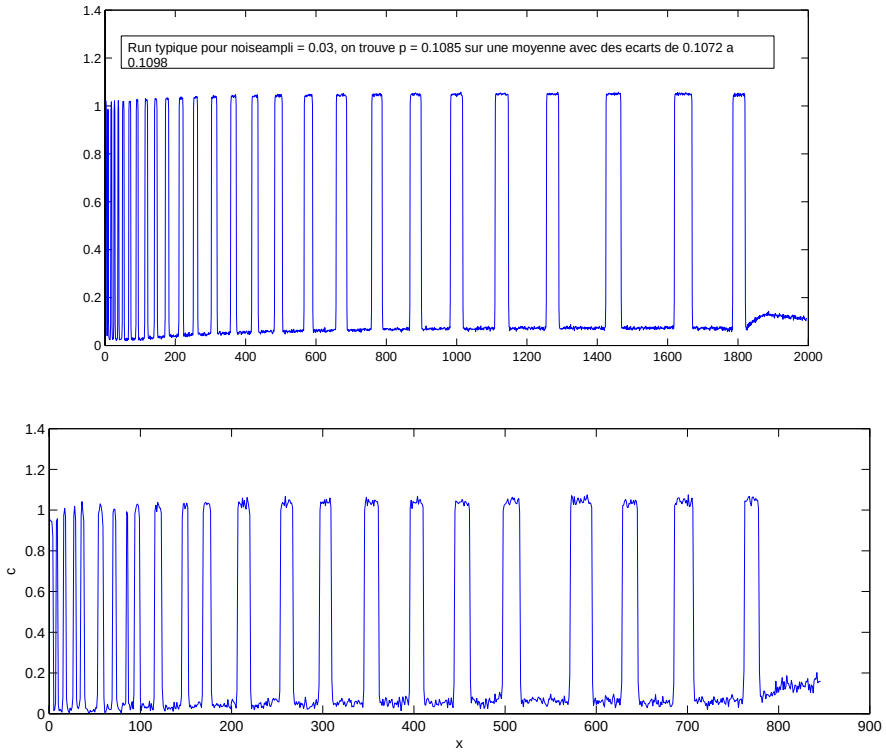

Figure 5.5: Banding obtained for the same parameter values as in Fig.(5.1) but with : (a) Weak noise $N_{ampli} = 0.02$, the spacing law is still a good approximation. (b) Stronger noise $N_{ampli} = 0.12$, irregularities appear.

values of p involved in the spacing law $x_n = Q(1+p)^n$ as a function of the noise amplitude. The effect could equivalently have been taken into account in the amplitude Q.

The decrease in p seems to be linear with the noise-amplitude. In order to explain this, let's return to the expression of the Matalon-Packter law as derived in Chap.2, (2.10) or (2.6):

$$p = 1 + c^* \alpha \tag{5.12}$$

where c_s plays the role of c^* in the spinodal decomposition scenario, α is a constant depending on the diffusion coefficients. As explained, when the front comes within $\sqrt{\langle \nu^2 \rangle}$ of c_s, a fluctuation is very likely to trigger the precipitation. We can thus say there is an effective threshold $\tilde{c_s} = c_s - \sqrt{\langle \nu^2 \rangle}$. Inserting this last expression in (5.12), we get the linear decrease of $\tilde{p}$ with

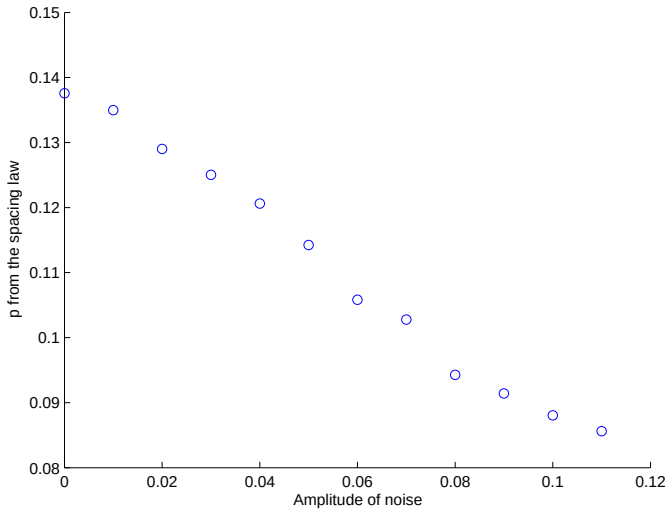

Figure 5.6: The spacing coefficient p of the width-law as a function of the noise intensity N_{ampli}. The decrease is linear.

the noise intensity.

Moderate noise and equidistant patterning

Although the following result is quite descriptive, it is interesting to quote it in relation with the discussion of (5.1.2). We see in Fig.(5.7) that the noise dramatically accelerates the onset of the instability. For a same amount of time, the number of bands created in the noisy case is about twice as much as in the noiseless one. The characteristic wavelength λ is still visible, but we expect the system to arrive much earlier in the regime where the diffusion front dictates the evolution time of the system, since the instability moves on more quickly in the presence of noise and will thus reach the front earlier than in the absence of noise. This would tend to emphasize that the equidistant patterning regime is transient and hardly observable on reasonable (long enough) length-scales.

Moderate noise : the nucleation regime

The profile shown in Fig.(5.8) shows a regime which is purely noise-induced : the concentration left by the front is too low to trigger spinodal decomposition. However, local sporadic fluctuations which exceed the critical radius

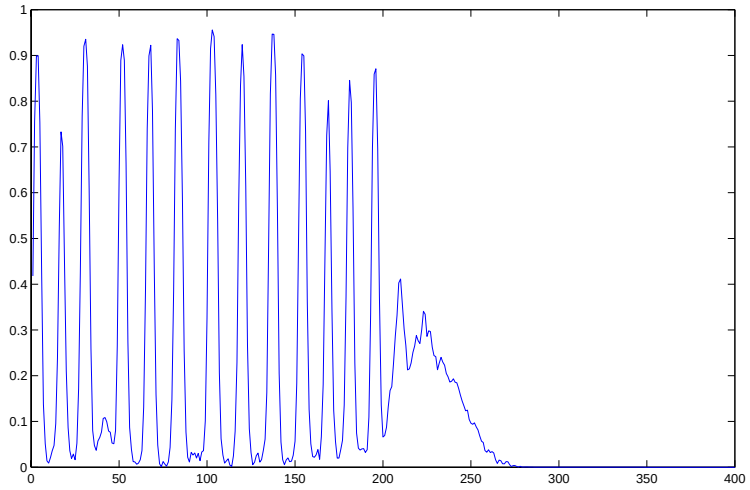

Figure 5.7: Exactly the same simulation as presented in Fig.(5.3) but with a noise $N_{ampli} = 0.03$. The number of bands formed in the same time interval has almost doubled !

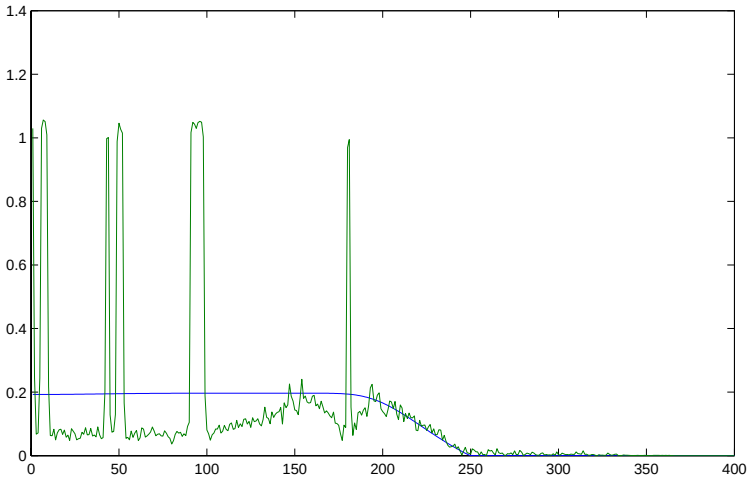

Figure 5.8: In this regime, the concentration deposited by the front is just below the spinodal. Without noise, one would observe a constant density of C's, indicated by the blue line. Here, local fluctuations induce sporadic precipitation, leading to a highly irregular pattern.

induce precipitation (if they are subcritical, they are "swallowed" by the surroundings according to the simulations of Chap.4). We believe that this behaviour is at the origin of irregular patterning as observed in Fig.(5.9). Note that this experiment was performed with an initially homogeneously supersaturated gel. An experiment performed by P.Hantz on the CuOH system but with the usual Liesegang initial conditions also reports irregular patterning, which could be explained by our model as well.

5.2.3 Two dimensional case

The next step towards gaining insight in the effect of stochasticity on Liesegang patterns is to consider two dimensional systems. Our hope is to reproduce some of the typical defects listed in Fig.(1.4).

We concentrated on ring-like systems, ie, which have an axial symmetry in the absence of noise. The role of noise is then precisely to break this symmetry and give the spiral's twirl, for example.

Let us consider one by one the modifications which have to be applied to the model to make it two-dimensional.

The source in polar coordinates

In Chap.3, we derived the scaling exponents of the source for a 1D problem consisting of an infinite reservoir of A on the left hand-side and of B on the right hand side with $a_0 \gg b_0$. How are those coefficients modified in the case where a disk-like drop of A is placed on a plane with B ?

The equations are the by-now usual reaction-diffusion equations (3.5). Let us first discuss the boundary conditions of the problem. Let D be the disk of radius r_0 at the center of the system (the drop), $\bar{D}$ its complementary. If

$$\begin{cases} a(D, t=0) = a_0 \\ b(\bar{D}, t=0) = b_0 \\ b(r=\infty, t) \to b_0 \end{cases} \tag{5.13}$$

then the problem obviously will not show any scaling behaviour. In fact, A diffuses and reacts outwards until so little of it is left that the front actually changes direction and eats up any remaining A. We thus have to consider a situation where A is continuously fed to the system :

$$\begin{cases} a(D,t) = a_0 \\ b(\bar{D}, t=0) = b_0 \\ b(r=\infty, t) \to b_0 \end{cases} \tag{5.14}$$

Experiments corresponding to these boundary conditions were shown earlier, see Fig.(1.3).

There again, we don't expect any scaling behaviour since a length-scale appeared, r_0. Indeed, if the solution were of the form $f(\frac{r}{\sqrt{t}})$, its value at the boundary would be $f(\frac{r_0}{\sqrt{t}})$ which varies with time in contradiction with (5.14).

So it is not mathematically obvious that $x_f \propto \sqrt{t}$. In analogy with the calculation done by [23], we tried solving for $u = a - b$ which obeys the simple diffusion equation :

$$\begin{cases} u(r,t) = \frac{1}{r}\frac{\partial}{\partial r}(r\frac{\partial}{\partial r}) \\ u(r_0, t=0) = a_0 \\ u(r=\infty, t) \to -b_0 \end{cases} \tag{5.15}$$

With the conditions (5.13), everything can be solved easily by Green's function. But (5.14) contains an astringent boundary condition which makes a similar approach impossible. The method of images fails because we are on $r \in [r_0, \infty]$. Laplace transformation (in r) stumbles upon unsatisfiable boundary conditions for $\tilde{u}(s,t)$. Turning to separation of variables poses the problem of finding an orthonormal set of functions on $[r_0, \infty]$. We dot not know (despite fierce efforts) whether this problem has any simple analytic solution.

In lack of analytical credit, we turn to the computer. Solutions of equations 3.5 for an infinite reaction rate indicate that :

- $r_f(t) \propto \sqrt{t}$
- $R \propto t^{-1/2}$

We conclude that the front in polar coordinates can, for practical purposes at least, be well described by the same source term that was used in the 1D simulations, where we replace $x \to r$.

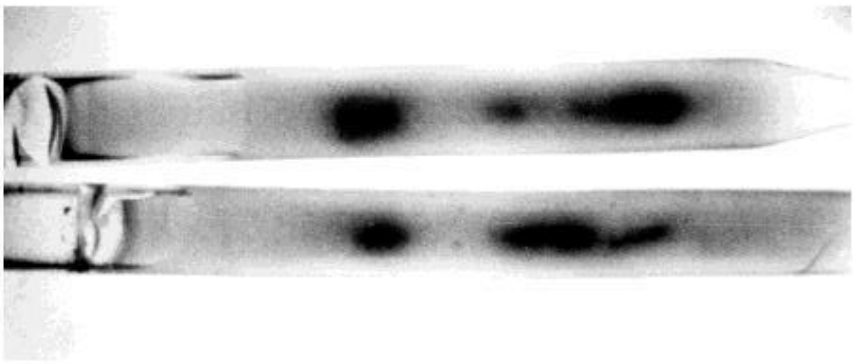

Figure 5.9: Inhomogeneous macroscopic structures formed from initially homogeneous supersaturated solutions of lead iodide in agar gel. Initial concentrations: 4.53 mM Pb(NO3)2, 18.07 mM KI. Tube diameter, 5 mm.

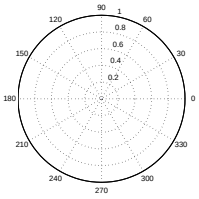

Figure 5.10: Grid used for the 2D simulations.

The grid

In order to respect the initial symmetry of the system, we adopted a polar-coordinate grid, that is, one where the radius r and the angle $\phi \in [0, 2\pi]$ are discretized (see Fig.(5.10)).

Implementation of the initial, boundary (no-flux) conditions and source data is made trivial by such a choice. Unfortunately the surface element grows linearly with r in this system. We thus have to fix some desired definition of the angular step Δ_ϕ at the maximum radius r_{max}. But Δ_ϕ will then be very small at the initial radius r_{ini}, which can lead to numerical instabilities unless the time step satisfies :

$$\Delta t < \frac{cste}{\Delta x^2} \tag{5.16}$$

which is a upper limit on the time-step and consequently the computing-time.

Model B in polar coordinates

Since we don't expect any qualitative changes between the deterministic behaviours of Model B' and Model B and since the latter can be implemented more easily, we decided to make use of it in a first try. The order parameter used is $\rho = 2c-1$ which admits the equilibrium states $c_l = 0$ and $c_h = +1$.

The gradient and laplacian in polar coordinates being given by,

$$\nabla = \frac{\partial}{\partial r}\vec{e_r} + \frac{1}{r}\frac{\partial}{\partial \phi}\vec{e_\phi}$$

and

$$\triangle = \frac{\partial^2}{\partial r^2} + \frac{1}{r}\frac{\partial}{\partial r} + \frac{1}{r^2}\frac{\partial^2}{\partial \phi^2}$$

we can express (4.33) as :

$$\dot{c}(r,\phi) = -(\underbrace{R(r)}_{\substack{purely \\ radialpart}} + \underbrace{\Phi(r,\phi)}_{\substack{mixed \\ part}}) \tag{5.17}$$

where

$$\begin{aligned} R &= \left(\frac{\partial^2}{\partial r^2} + \frac{1}{r}\frac{\partial}{\partial r}\right)\left(\epsilon\rho - \gamma\rho^3\right) \\ &\quad +\sigma\left(\frac{1}{r^3}\frac{\partial \rho}{\partial r} - \frac{1}{r^2}\frac{\partial^2 \rho}{\partial r^2} + \frac{2}{r}\frac{\partial^3 \rho}{\partial r^3} + \frac{\partial^4 \rho}{\partial r^4}\right) \end{aligned} \tag{5.18}$$

and

$$\begin{aligned}\Phi &= \frac{1}{r^2}\frac{\partial^2}{\partial\phi^2}\left(\epsilon\rho-\epsilon\rho^3\right)\\ &\quad+\sigma\left(\frac{2}{r^2}\frac{\partial^4\rho}{\partial\phi^2\partial r^2}-\frac{2}{r^3}\frac{\partial^3\rho}{\partial\phi^2\partial r}+\frac{1}{r^4}\frac{\partial^4\rho}{\partial\phi^4}+\frac{4}{r^4}\frac{\partial^2\rho}{\partial\phi^2}\right)\end{aligned} \tag{5.19}$$

We describe how the multiplicative-noise term was treated and discretized in Appendix C.

Results in the noiseless case

The problem is effectively one-dimensional (radial) in this case. The equation obeyed by the system is given by (5.18).

The behaviour is similar to that observed in the 1D case. An important difference is that the rings are not stable at very long times. In fact, a ring is composed of an inner and outer interface. In order to minimize its surface tension, it should minimize its surface while keeping the C that is in it constant : the energetically favorable solution is clearly to collapse to a disk (with just one interface). So the rings tend to get closer to the center. This is shown in Fig.(5.11) where one sees that there is "one band less" in the right picture although it was shot later. This process is slow and concerns mainly the bands in the vicinity of the center of the system; it is nevertheless a somewhat troubling facet of Model B since such behaviour was not, to our knowledge, experimentally observed.

Results in the noisy case

Fig.(5.12) shows a typical result of noisy Liesegang rings obtained in our model. The first ring presents two gaps (which may still close up after some coarsening), while at the outskirts, nucleation randomly promotes some spots in the haze of the front to precipitate form. Unfortunately, we had very little time to thoroughly browse through the parameters of this 2D simulation (ie noise intensity, ϵ, σ ...). Also, the maximal radius being rather limited with this grid, large-scale and long-time simulations are practically impossible. This puts one in a position to wonder if a very fine cartesian grid, albeit uncomfortable for the implementation of boundary conditions, wouldn't have been a better compromise.

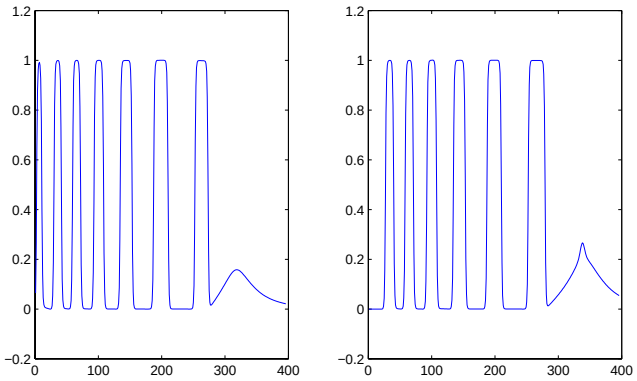

Figure 5.11: Simulation of Model B with source in polar coordinates, without noise. The problem is then effectively radial. The picture to the right is shot later than the one to the left, but it contains fewer bands. This indicates that the first bands underwent coarsening, coagulating to form only one band.

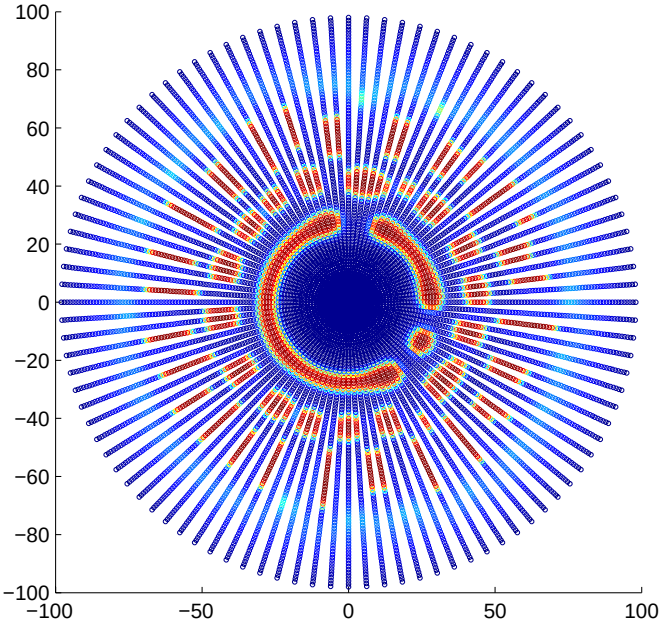

Figure 5.12: Results obtained for a 2D simulation of Model B' with noise. The radial lines is the grid, which shouldn't be visible ! The resolution is thus acceptable just for the 1-2 first rings.

Chapter 6

Liesegang patterns in electric fields

The effect of an electric field on 1D LE has been studied experimentally as well as theoretically ([28]). In Fig.(6.1), we depict the archetype setup for such experiments. The main experimental results were summarized in Chap.1. Electric fields act only the charged species. The dynamics of the colloid suspension C is thus supposed to be unaffected by the field. The only change which can occur is in the source term $S(x,t)$. We will quickly review the modifications induced on the reaction front ([29]) by the ionic nature of the species and the electric field, as well as their consequences for LP. In the final part we consider the special case where the precipitation reaction involves bivalent ions. No significant departure from the monovalent ion case is found.

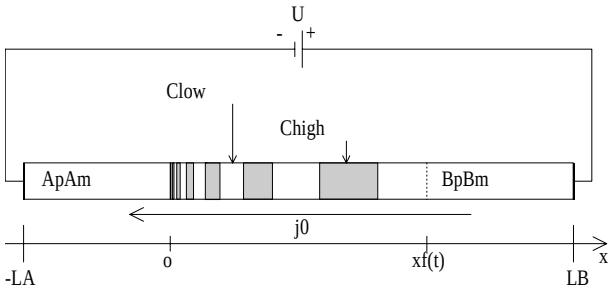

Figure 6.1: LE in eletric field. The *direct field* case pushes the reacting A^- and B^+ towards the reaction zone, while the *revert field* drags them away.

6.1 No electric field : effect of charges in the case of different diffusion constants

The reaction we consider is

$$A^- + B^+ \rightarrow C \tag{6.1}$$

The initial conditions are the same as in the usual LE, but *no electric fields are present* (yet). The system is locally electroneutral up to a distance r_D. This leads to an important feature in the case of unequal diffusion constants for the ions, say D_- for A^-, D_+ for A^+ and $D_- > D_+$. Indeed, the A^- ions, responsible for the creation of the front, are slowed down by their counterpart A^+. Local electric fields appear, though the overall system is electroneutral [24]. This can be formulated mathematically in introducing an electric field component $E(x,t)$ in the equations for the current density of the ionic species:

$$j_i = -D_i(\frac{\partial n_i}{\partial x} - E(x,t)n_i z_i/\phi_0) \tag{6.2}$$

where i indexes the various species present, z_i their electric charges, and $\phi_0 = RT/F$ (R is the gaz constant, T the temperature and F the Faraday constant). The electric field induced can be derived by the electroneutrality condition and a continuity equation for each of the species :

$$E(x,t) = \frac{\sum_i z_i D_i \frac{\partial n_i}{\partial x}}{\sum_i z_i^2 D_i n_i} \tag{6.3}$$

Without going into details, the effect can be shown to generate an effective modification of the diffusion constant of the front (it is slowed down in the example we discussed above) and of the behind-the-front concentration c_0, but does not induce any new qualitative effects. It is however instructive to see how forces can be generated in a system in the absence of electric fields, and strongly narrows the validity of D_f given as in (3.10) to species having approximately the same diffusion constants.

6.2 Effect of an applied electric field on the front motion

The calculation of the modification induced by a a fixed external electric field [29] being mainly numerical, we consider it sufficient to give here just a brief summary of the main new physical effects:

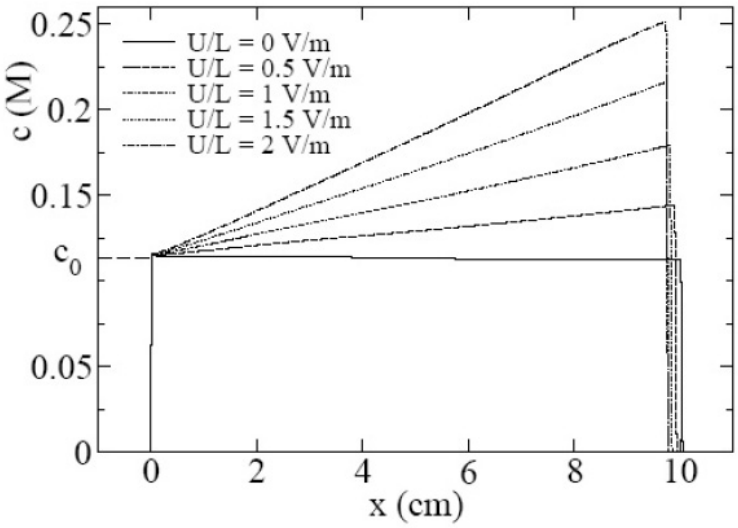

Figure 6.2: Values of the behind-the-front concentration of C's for different values of the applied electric field.

In the case of a forward applied field, that is when the A^- and B^+ ions are pushed towards the reaction zone by the field.

1. The motion stays diffusive and D_f is slightly lower than in the fieldless case. This can be understood in the following way : in order to ensure local electroneutrality, the A^+ must accompany the A^- ions which gradually transform into C. However, this motion is made *against* the electric field, which thus slows down the overall motion of the front. The argument holds for the B^- ions as well.

2. The most important new feature is that the concentration left behind the front is no more constant but increases linearly (Fig. 6.2) with x.

   The proportionality coefficient is related to the intensity of the applied field $\approx U/L$:

   $$c(x) = c_0(1 + (\alpha U/L)x) \tag{6.4}$$

   This can be understood by the fact that the potential difference generates a current in the system, in addition to the diffusive one. It is seen numerically that this current is almost constant in time, its value

being dictated by the resistance of the gel column essentially, and only very slightly modified by the evolution of the depletion zone around the reaction front. Including this fact, the argument from Chap.3 concerning the constancy of the deposited concentration can be repeated and we find $c(x_f)$ as the sum of two parts, one proportional to x_f and the other constant.

6.3 LP in electric fields

The result (6.4) on the spatial dependence of the concentration of the reaction product in presence of an applied electric field is incorporated into the source term through the following modification of its amplitude :

$$S_m(x,t) = a_0 \frac{K\sqrt{D}}{(ch-cl)/2}[1+(\nu U/L)x]\frac{\delta(x-xf(t))}{\sqrt{t}} \tag{6.5}$$

Here the moving front is considered as point-like. The solution to Model B with this modified source is obtained numerically, see Fig.(6.3).

A first generic feature of the patterns formed in the presence of the forward field ($U > 0$ in this setup) is that the number of bands is finite, i.e., band formation stops at a certain moment through the appearance of a continuous precipitation region (a "plug" of high-density precipitate). The higher the tension, the earlier this plug forms.

A second generic feature of the pattern is that the distance between two successive bands diminishes as compared to the fieldless case, and this effect is increasing with increasing forward applied field U/L. This can be easily understood through a simple qualitative argument. In the presence of the forward field, the reaction front leaves behind a larger quantity of C than in the absence of the field. Thus, after the formation of a band, the re-establishment of the phase-separation instability conditions takes place sooner in the presence of the field, resulting in a higher spatial density of bands in the system. We thus recover the experimental results presented in the Chap.1.

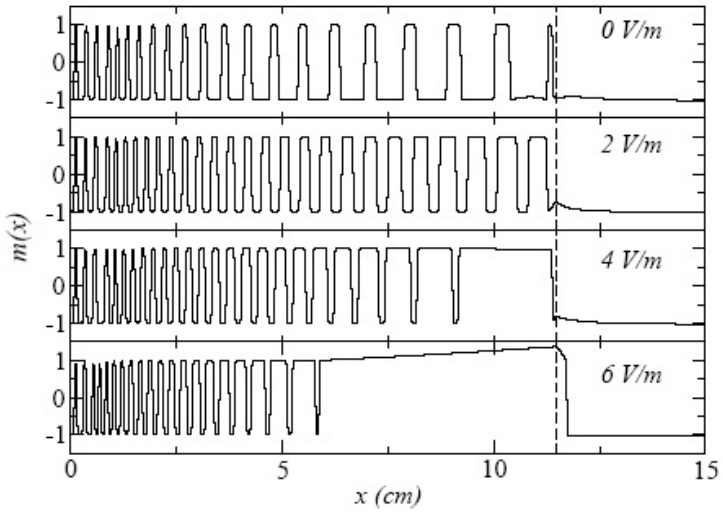

Figure 6.3: The profile of the concentration $c(x)$ for different values of the forward applied field $U/L > 0$. The snapshots are taken at $t = 14$ days. The dashed lines represent the position of the reaction front at this time. One notices the decrease in the band spacing with increasing tension, as well as the appearance of the plug – earlier for larger tensions.

6.4 The influence of bivalent ions

This study is motivated by the fact that the results obtained in the frame of the spinodal decomposition scenario in electric fields ([28]) agree with all experimental studies except the one by Lagzi [15]. In the latter, the spacing coefficient is found to increase with increasing forward field. The time of formation of each band is also found to deviate strongly from the square root law. The stoechiometry of the precipitation reaction in this experiment is

$$2Ag^{+} + Cr_2O_7^{2-} \rightarrow (Ag)_2Cr_2O_7$$

while the theoretical work [29] considers just the case

$$A^{-} + B^{+} \rightarrow C \tag{6.6}$$

Taking into account the exact stoechiometry of the ions could be responsible for this deviation from experiment. We present in Fig.(6.6) and Fig.(6.9) comparative graphs of the monovalent and bivalent ion case. Parameter values are : $a_0 = 10$ M; $b_0 = 0.2$ M, $L_A = 20$ cm; $L_B = 50$ cm , $time = 10$ days, $U/L = -10$ V/m for forward field, $U/L = +1$ for reverse field, infinite reaction rate and $D = 10^{-9}$ m^2/s for all species.

The deviation from the monovalent case is very scarce. The most important point is that the profile of C deposited is increasing linearly in both cases, and with nearly the same slope. Taking this slight modification into the source for Model B obviously will not bring about any consequent modifications in the observed banding, and certainly not the reverse behaviour observed by [15].

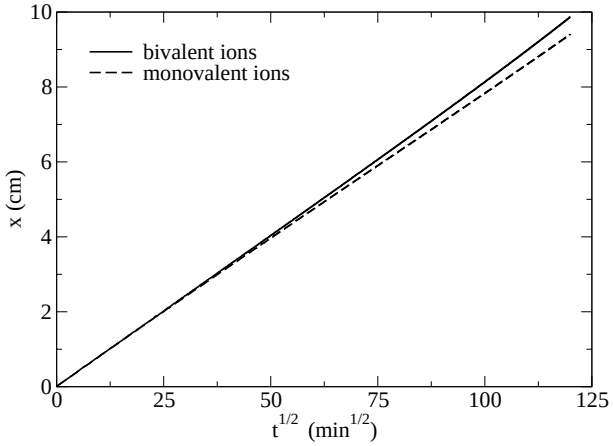

Figure 6.4: Forward field : position of the reaction diffusion front as a function of time

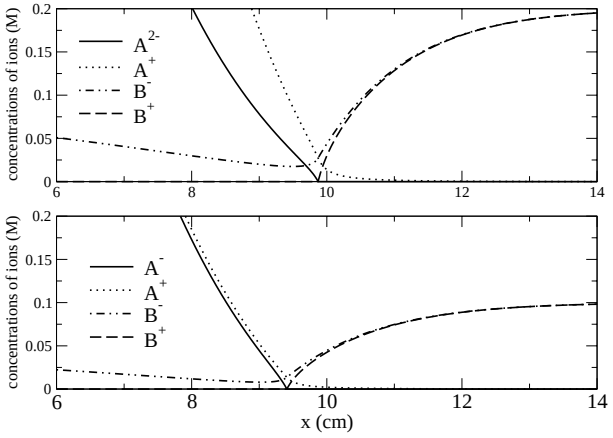

Figure 6.5: Forward field : concentration of the ions in the system at 10 days.

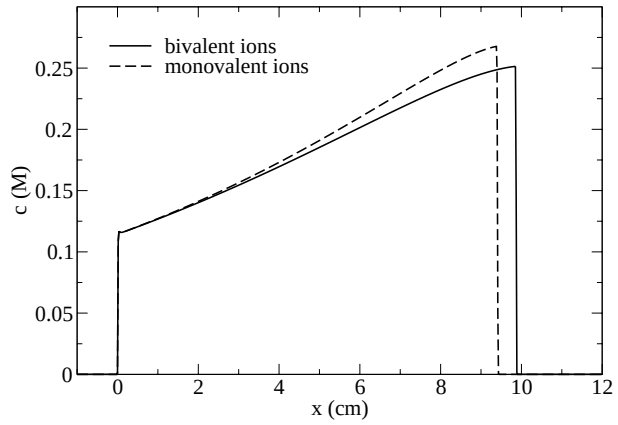

Figure 6.6: Forward field : concentrations of the precipitate deposited at 10 days.

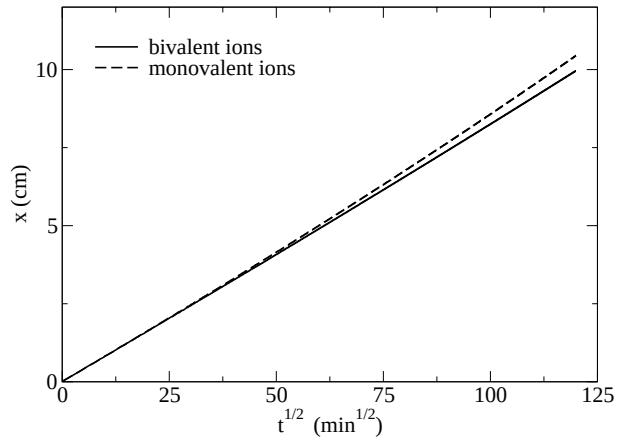

Figure 6.7: Reverse field : position of the reaction diffusion front as a function of time

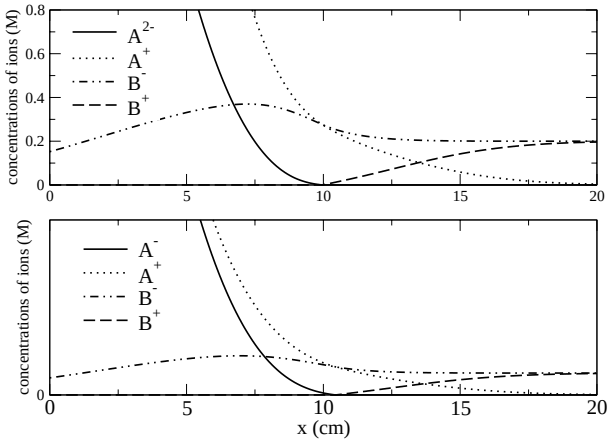

Figure 6.8: Reverse field : concentration of the ions in the system at 10 days.

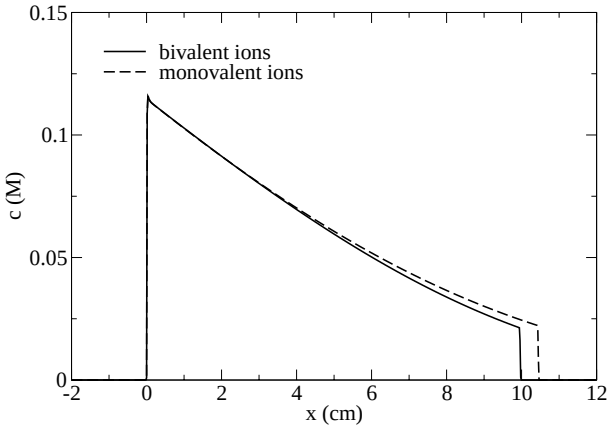

Figure 6.9: Reverse field : concentrations of the precipitate deposited at 10 days.

Chapter 7

Conclusions and outlooks

Liesegang rings have been able to grab the fancy of scientists for over a hundred years. The amount of papers related to it surpasses all possible expectations : one reports more than 1500 references ! Theories of LP formation are numerous and the basic experimental facts are by now understood. However, while some theories (like ours) do present overall better features than others, none of them can possibly handle all the variations (presented in Chap.1) and stray behaviours to which Liesegang systems are prone. Such a theory would have to take in account too much parameters and involve tedious, breathtaking, not to say time-wasting computer simulations ; fascination towards LPs is, we believe, like a mine vein : it lasts a while, but inevitably becomes exhausted.

The author supports the standpoint, that for Liesegang science to further develop, it is in dreadful need of applications. Some research groups (from which the above philosophy was - at least partially - borrowed) have started going this way ([20]), shrinking the size of single rings to the so-much-yearned-for nano-scale. If LPs were to appear as an essential part of some industrial process and one could, leaning back in a leather armchair, proudly announce to startled visitors "that, my dear, was produced by Liesegang technology", then this would definitely trigger a revival of interest towards them.

Appendix A

Ito and Stratonovich conventions

We explicit here the origin of the ambiguity concerning the interpretation of multiplicative noise. We also give formulas for changes of variables in stochastic differential equations (SDEs). [37] gives a complete introduction to stochastic calculus.

Averaging of the noise

Let's keep aside for a while the deterministic part of the evolution of $c(x,t)$ and see what dynamics the noise induces. We generalize the term $\sqrt{c(x,t)}$ to a more general function $g(c(x,t))$.

$$\dot{c}(x,t) = \nabla(g(c(x,t)\xi(x,t))$$

By formal integration over a small time interval Δt, we get :

$$c(x,t+\Delta t) = c(t) + \nabla \int_t^{t+\Delta t} g(c(x,t'))\xi(x,t')dt'$$

We now wish to take the average over the realizations of the noise.

- According to Ito's convention, $g(c(x,t'))$ can be replaced by it's value at t. Thus,

$$c(x,t+\Delta t) = c(t) + \nabla g(c(x,t)) \int_t^{t+\Delta t} \xi(x,t')dt'$$

Since $\langle \xi(x,t) \rangle = 0$, this yields

$$\langle c(x,t+\Delta t)\rangle = \langle c(x,t)\rangle$$

So multiplicative noise doesn't induce any dynamics for the average concentration in Ito's convention.

- According to Stratonovich, $g(c(x,t'))$ has to be evaluated in the middle of the interval of integration, that is at $t' = (t + \frac{\Delta t}{2})$

$$c(x,t+\Delta t) = c(t) + \nabla \int_t^{t+\Delta t} g(c(x,t+\frac{\Delta t}{2}))\xi(x,t')dt' \qquad (A.1)$$

To continue, we have to expand $g(c(x,t+\frac{\Delta t}{2}))$ in a Taylor series,

$$\begin{aligned} g(c(x,t+\frac{\Delta t}{2})) &\approx g(c(x,t)) + \frac{\Delta t}{2}\frac{\partial c}{\partial t}\frac{\partial g(c)}{\partial c} \\ &= g(c(x,t) + \frac{\Delta t}{2}\nabla(g(c(x,t))\xi(x,t))\frac{\partial g(c)}{\partial c} \end{aligned} \qquad (A.2)$$

We already get a glimpse of what is happening : by replacing (A.2) in (A.1), the correlation function of ξ appears, which has a non-zero average,

$$\begin{aligned} \langle c(x,t+\Delta t)\rangle &= \langle c(t)\rangle + \langle \nabla \int_t^{t+\Delta t} \frac{\Delta t}{2}\nabla(g(c(x,t))\xi(x,t))\xi(x,t')\frac{\partial g(c)}{\partial c}\rangle \\ &= \langle c(t)\rangle + \frac{\Delta t}{2}\nabla(\frac{\partial g(c)}{\partial c}\nabla g(c))2D \end{aligned} \qquad (A.3)$$

We see that in the Stratonovich convention, noise does induce some dynamics. If we take $g(c) = \sqrt{c}$, we get

$$\dot{c} = \frac{D\Delta t}{2}\nabla\left(\frac{\nabla c}{c}\right) \qquad (A.4)$$

a fairly pathological result since it blows up for $c \to 0$.

Let's note that the result (A.3) is a particular case of Novikov's theorem:

$$< \xi(x,t)g(\xi) >= \int dt' \int dx' K(x-x')C(t-t')\langle \frac{\delta g(\xi)}{\delta \xi(x',t')}\rangle \qquad (A.5)$$

where $\xi(x,t)$ is a gaussian noise with correlation

$$\langle \xi(x,t)\ \xi(x',t') \rangle \ = \ K(x-x')\ C(t-t')$$

. (A.5) can be brought to the form of (A.3) by noting that

$$\frac{\delta g(\xi)}{\delta \xi(x',t')} = \frac{\delta g(c(\xi))}{\delta c} \frac{\delta c}{\delta \xi(x',t')} = g'(c) \frac{\delta c}{\delta \xi(x',t')} \tag{A.6}$$

Change of variable

Be the stochastic equation with gaussian noise

$$\dot{X} = a(X) + b(X)\eta$$

$$\langle \eta(t)\eta(t') \rangle = 2D\delta(t-t')$$

and a function $f(X)$, with $\nabla f = df/dX$.

- Ito's formula for a change of variable is

$$\frac{df(X)}{dt} = (a(X)\nabla f + D\nabla^2 f) + \eta \nabla f$$

- Stratonovich's formula for a change of variable is

$$\frac{df(X)}{dt} = (a(X) + \eta)\nabla f$$

We can apply these results to the derivation of Model B'; that is done in Appendix B.

Appendix B

Derivation of Model B'

Starting off with

$$\dot{X}_i(t) = \xi_i(t) - \frac{1}{\kappa}\sum_{j=1}^{N} \nabla V(X_i(t) - X_j(t))$$

$$\langle \xi_i(t)\xi_j(t)\rangle = 2D\delta_{ij}\delta(t-t')$$

We want to derive an equation for

$$\rho(x,t) = \sum_{i=1}^{N} \delta(X_i(t) - x) = \sum_{i=1}^{N} \rho_i(x,t)$$

Using the Stratonovich rule for a change of variable, we have, for an arbitrary function $f(x)$:

$$\frac{df(X_i)}{dt} = \left[\sum_{j=1}^{N} \nabla V(X_i(t) - X_j(t)) + \xi_i(t)\right] \nabla f(X_i)$$

where we absorbed $1/\kappa$ in the potential. We can also write

$$\frac{df(X_i)}{dt} = \int dx \rho_i(x,t) \left[\sum_{j=1}^{N} \nabla V((x) - X_j(t)) + \xi_i(t)\right] \nabla f$$

by integration by parts (with $\rho \mid_\infty = \frac{\partial \rho}{\partial x} \mid_\infty = 0$), and rewriting

$$\frac{df(X_i)}{dt} = -\int dx f(x) \nabla \left[\rho_i(x,t) \sum_{j=1}^{N} \nabla V((x) - X_j(t)) + \rho_i(x,t)\xi_i(t)\right]$$

On the other hand, we have

$$\frac{df(X_i)}{dt} = \int dx \frac{\partial \rho_i(x,t)}{\partial t} f(x)$$

and since these expressions are valid for any function $f(x)$, we get, by summing over all particles,

$$\frac{\partial \rho}{\partial t} = \sum_{i=1}^{N} \nabla \left(\xi_i \rho_i(x,t) \right) + \nabla \left(\rho(x,t) \int dy \rho(y,t) \nabla V(x-y) \right) \tag{B.1}$$

This is almost the expression obtained in 4.24, up to the $\nabla^2 \rho$ term. This term has it's origin in Ito's formula for the change of variable. In this calculation, we will recover it by calculating the average of the noise term. According to the results of Appendix A, we have :

$$\langle \sum_i \nabla(\rho_i(x,t)\xi_i(t)) \rangle = -T\nabla \sum_i \nabla_x \rho_i(x,t) = -T\nabla^2 \rho(x,t)$$

This is exactly the term we were looking for. The morale of all this is that, starting from a well defined equation with additive noise, both conventions lead to the same results, whichever the mathematical manipulations being performed in between.

Appendix C

Numerical procedure for 2D simulations

By symmetric finite-difference method, we get a discrete form of equations (5.18), (5.19). We take no-flux boundary conditions for the radial variable and of course periodic ones for the angle ϕ.

How does the noise term transform ?

We simply have

$$\nabla(\sqrt{c}\xi) = \frac{\partial(\sqrt{c}\xi)}{\partial r}\vec{e_r} + \frac{1}{r}\frac{\partial(\sqrt{c}\xi)}{\partial \phi}\vec{e_\phi}$$

ξ is now a 2 component vector. We know that, upon discretization, we have to replace the delta functions of the correlation function of the noise by

$$\begin{aligned} \delta(r) &\to \Delta r \\ \delta(\phi) \to \Delta\phi(r) &= \frac{2\pi r}{N_\phi} \end{aligned} \tag{C.1}$$

Since this is in the mean square of the noise, we have to take the square root and the term $\nabla(\sqrt{c}\xi)$ is equivalent to adding at each iteration :

$$\begin{aligned} &\sqrt{\frac{2\pi r\Delta t}{N_\phi \Delta r}}\frac{\eta_{i+1,j}\sqrt{c_{i+1,j}} - \eta_{i-1,j}\sqrt{c_{i-1,j}}}{2} \\ &\sqrt{\frac{2\pi \Delta t}{N_\phi}}\frac{\eta_{i,j+1}\sqrt{c_{i,j+1}} - \eta_{i,j-1}\sqrt{c_{i,j-1}}}{2} \end{aligned} \tag{C.2}$$

where (i, j) denotes the discretized pair (radius, angle). Δt, Δr, N_ϕ, η are respectively the time step, radius step, total number of subdivisions of 2π and a gaussian random variable.

Bibliography

[1] K.Kang, S.Redner, PR A 32 1, 1985, *Fluctuation-dominated kinetics in diffusion-controled reactions*

[2] P.L.Krapivsky PR E 51 5, 1995, *Diffusion-limited annihilation with initially separated reactants*

[3] D.Toussaint,F.Wilczek J.Chem.Phys 78(5), 1983, *Particle-antiparticle annihilation in diffusive motion*

[4] J.Magnin, PhD thesis, *Pattern Formation in Reaction-Diffusion Systems : the Liesegang Structures*

[5] G.T.Dee, PRL 57 3, 1986, *Pattern produced by precipitation at a moving reaction front*

[6] A.J.Archer, R.Evans, J.Chem.Phys. 121 9, 2004, *Dynamical density functional theory and its application to spinodal decomposition*

[7] N.G. Van Kampen, J. Stat. Phys. 24, 175 (1981).

[8] J. Langer, Ann. Phys. 65, 53 (1971).

[9] B. Chopard, P. Luthi, M.Droz PRL Vol. 72(1994), no 9, p. 1384-1387, *Reaction-diffusion cellular automata model for the formation of Liesegang patterns*

[10] H-J.Krug, H.Brandstaedter, J.Phys.Chem. A 103 7811-7820, 1999, *Morphological characteristics of Liesegang rings and their simulation*

[11] J. Garcia-Ojalvo, J.M.Sancho, *Noise in spatially extended systems* Springer

[12] I.Daruka, J.Tersoff, PRL 95, 076102 (2005) *Self-assembled superlattice ny spinodal decomposition during growth*

[13] R.Feeney, P.Ortoleva et al. J Chem. Pys. 78(3) 1983 *Periodic precipitation and coarsening waves : applications of the competitive particle growth model*

[14] J.M.Sancho et al. Phys. Rev. B 48, 119124 (1993) *Fluctuations in domain growth: Ginzburg-Landau equations with multiplicative noise*

[15] I.Lagzi J. Phys. Chem. 4, 1268 (2002) *Formation of Liesegang patterns in an electric field*

[16] D.S.Dean, J.Phys A : Math. Gen., 1996 *Equation of motion for the density of interacting brownian particles*

[17] N.R.Dhar, A.C.Chatterji J. Phys. Chem. 28, 41 5.2

[18] J.Obrist , Colloid and Polymer Science (Springer), 1937

[19] R. E. Liesegang, Naturwiss. Wochenschr. **11**, 353 (1896).

[20] Fialkowski, Bitner, Grzybowski, Phys. Rev. Lett., vol. 94, Issue 1, id. 018303.

[21] T.Kosztolowicz et al. cond-mat/0504261 Apr. 2005 *How to measure subdiffusion parameters*

[22] S. Cornell, M. Droz Phys. Rev. Lett. 70, 38243827 (1993).

[23] L. Gálfi and Z. Rácz, Phys. Rev. A **38**, 3151 (1988), *Properties of the reaction front in an A+B → C tpe reaction-diffusion process.*

[24] T. Unger and Z. Rácz, Phys. Rev. E **61**, 3583 (2000).

[25] T. Antal, M. Droz, J. Magnin, and Z. Rácz, Phys. Rev. Lett. **83**, 2880 (1999).

[26] M. Droz, J.D Gunton, "*An introduction to metastable and unstable states", Springer Verlag, Monographs in Physics.*

[27] J. D. Gunton, M. San Miguel, and P. S. Sahini, in *Phase Transitions and Critical Phenomena*, Vol. 8, *The Dynamics of First-order Transitions*, Eds. C. Domb and J. L. Lebowitz (Academic Press, New York, 1983).

[28] I. Bena, M. Droz, and Z. Rácz, J. Chem. Phys.(2005).

[29] I. Bena, F. Coppex, M. Droz, and Z. Rácz, J. Chem. Phys. **122**, 024512 (2005), *Front motion in an A+B ... : Effects of an electric field*

[30] T. Antal, M. Droz, J. Magnin, A. Pekalski, and Z. Rácz, Journal of Chemical Physics **114**, pp. 3770–3775 (2001), *Formation of Liesegang patterns: Simulations using a kinetic Ising model*

[31] H.K Hennisch *Crystals in Gels and Liesegang Rings*

[32] P.Hantz, J. Phys. Chem. B 2000, 104, 4266-4272, *Pattern formation in the NaOH + CuCl2 Reaction*

[33] A.Toramaru et al. Physica D 183, 133-140, 2003, *Experimental pattern transitions in a Liesegang system*

[34] G.Venzl and J.Ross, J. Phys. Chem. A 2003, 107, 7997-8008, *Spatial Structure Formation in Precipitation Reactions*

[35] I.Hein, American Journal of Botany, 1929, *Liesegang phenomena in Fungi*

[36] A.Toramaru et al. Forma 6 (3), 247-266, 1991, *The Liesegang model of the Titus Bode law*

[37] Gardiner, Springer *Stochastic differential equations in physics and chemistry*